nature reviews cardiology

https://doi.org/10.1038/s41569-025-01127-0

Review article

Check for updates

Wearable blood pressure sensors for cardiovascular monitoring and machine learning algorithms for blood pressure estimation

Seongwook Min[1,8], Jaehun An[1,8], Jae Hee Lee[2,8], Ji Hoon Kim[1], Daniel J. Joe[3], Soo Hwan Eom[4], Chang D. Yoo[4], Hyo-Suk Ahn[5], Jin-Young Hwang[6], Sheng Xu[7], John A. Rogers[2] & Keon Jae Lee[1]

Abstract

With advances in materials science and medical technology, wearable sensors have become crucial tools for the early diagnosis and continuous monitoring of numerous cardiovascular diseases, including arrhythmias, hypertension and coronary artery disease. These devices employ various sensing mechanisms, such as mechanoelectric, optoelectronic, ultrasonic and electrophysiological methods, to measure vital biosignals, including pulse rate, blood pressure and changes in heart rhythm. In this Review, we provide a comprehensive overview of the current state of wearable cardiovascular sensors, focusing particularly on those that measure blood pressure. We explore biosignal sensing principles, discuss blood pressure estimation methods (including machine learning algorithms) and summarize the latest advances in cuffless wearable blood pressure sensors. Finally, we highlight the challenges of and offer insights into potential pathways for the practical application of cuffless wearable blood pressure sensors in the medical field from both technical and clinical perspectives.

Sections

[1]Department of Materials Science and Engineering, Korea Advanced Institute of Science and Technology (KAIST), Daejeon, Republic of Korea. [2]Querrey Simpson Institute for Bioelectronics, Northwestern University, Evanston, IL, USA. [3]Safety Measurement Institute, Korea Research Institute of Standards and Science (KRISS), Daejeon, Republic of Korea. [4]Department of Electrical Engineering, Korea Advanced Institute of Science and Technology (KAIST), Daejeon, Republic of Korea. [5]Department of Internal Medicine, Division of Cardiology, Uijeongbu St Mary's Hospital, College of Medicine, The Catholic University of Korea, Seoul, Republic of Korea. [6]Department of Anaesthesiology and Pain Medicine, SMG-SNU Boramae Medical Center, College of Medicine, Seoul National University, Seoul, Republic of Korea. [7]Department of Nanoengineering, University of California San Diego, La Jolla, CA, USA. [8]These authors contributed equally: Seongwook Min, Jaehun An, Jae Hee Lee. e-mail: keonlee@kaist.ac.kr

Key points

- Wearable blood pressure (BP) sensors utilize diverse sensing methodologies, including mechanoelectric, optoelectronic, ultrasonic and electrophysiologic technologies, that facilitate continuous cardiovascular monitoring.
- Various approaches, including pulse wave analysis, pulse wave velocity and arterial wall dynamics, as well as advanced machine learning and deep learning algorithms that build on these methods, are being explored to improve the accuracy of BP estimation in wearable cuffless BP sensors.
- Cuffless BP sensors still face obstacles in achieving clinical-grade reliability due to issues with sensor calibration, motion artefacts and placement accuracy.
- Further improvements in sensor materials and system integration are crucial for improving the accuracy and clinical applicability of wearable BP sensors.
- Comprehensive clinical trials are essential to validate the performance of wearable BP sensors and ensure compliance with established medical standards for broader adoption in health-care settings.

Introduction

High blood pressure (BP), also known as hypertension, occurs when the force of blood against the walls of the arteries is abnormally high. This condition usually has no noticeable symptoms but can suddenly lead to cardiovascular diseases, such as myocardial infarction, coronary artery disease and stroke[1–5]. BP is most commonly measured via an invasive arterial catheter (the gold standard for acute care) or using a non-invasive, cuff-based sphygmomanometer (for hypertension diagnosis and management)[6]. However, both methods are limited by their inability to continuously monitor BP levels, which can be influenced by factors such as stress, diet and exercise[7–14]. Continuous, non-invasive BP monitoring during daily activities and sleep is essential to provide valuable clinical information, including BP variability and cardiovascular risk assessment[15–17].

In the past decade, wearable biosensors have been developed to continuously measure biosignals, such as pulse waves[18–23], volumetric changes in blood (photoplethysmography (PPG))[24–28], ultrasonic signals[29–32] and electrocardiogram (ECG) data[33–36]. Taking into consideration the mechanical properties of human skin, numerous biomaterials have been designed to measure small biomedical signals via advanced technologies, including mechanoelectronic, optoelectronic, ultrasonic and electrophysiological devices. On the basis of the acquired biosignals, BP can be estimated non-invasively by applying established concepts that define the correlation between BP values and features related to pulse wave intensity and time domain, as well as features related to arterial diameter, such as pulse wave analysis (PWA), pulse wave velocity (PWV) and arterial wall dynamics.

Despite these remarkable advances in cuffless wearable BP sensor technology, non-invasive wearable BP sensors have not yet been widely implemented in clinical practice given their low accuracy and reliability, owing to the generation of unrefined pulse waveforms and ambiguous feature extraction during the BP estimation process[37–40]. An improvement in both the hardware[41–45] and software[46–51] for these wearable sensors is essential to address these challenges. With regard to the hardware, the development of sensors capable of acquiring highly sensitive signals under varying conditions, such as in the presence of motion artefacts, physiological changes and ambient noise, is crucial to improve device accuracy. For the software, the incorporation of machine learning (ML) techniques is imperative for automatic feature extraction, real-time analysis and continuous improvement in the accuracy of BP measurements. Furthermore, integrating artificial intelligence with cloud-based analytics platforms allows continuous updates and improvements to algorithms based on a wide range of collected data, improving the accuracy and reliability of these wearable BP sensors.

In this Review, we provide an in-depth understanding of the current progress in cuffless wearable BP sensors with regard to biosignal acquisition principles, BP estimation approaches and the latest advances in wearable BP sensor systems (Fig. 1). Furthermore, we highlight the future directions in the field of wearable BP sensors, focusing on issues such as sensor accuracy, system integration and clinical application to ensure their effectiveness both in daily use and in clinical settings.

Principles for biosignal acquisition

Biosignals, such as pulse waves, volumetric changes in blood (PPG), ECG traces and ultrasonic signals, are fundamental data sources for continuous, indirect BP estimation. Wearable BP sensors acquire these biosignals from various body regions using intrinsic properties such as mechanoelectric[52] (including piezoelectric[53] and triboelectic[54] pulse sensors, piezoresistive sensors[55], capacitive sensors[56], field effect transistors[57,58] and electrets[59]), optoelectronic[60], ultrasonic[61] and electrophysiological[62] (Tables 1 and 2). Current research on wearable BP sensors focuses on engineering materials with optimally deformable structures to ensure conformal attachment to the human body and improved sensor sensitivity, aiming to provide more accurate measurements of biosignals that are crucial for effective BP monitoring.

Mechanoelectric principles

The integration of mechanoelectric materials into cardiovascular monitoring systems in the past decade has enabled non-invasive and continuous cardiovascular monitoring. These materials convert mechanical energy into electrical energy, allowing the detection of subtle mechanical deformations or vibrations within the arterial system, such as pulse waves[63]. A diverse range of mechanoelectric materials, including piezoelectric, triboelectric, piezoresistive and capacitive materials, have been utilized in wearable BP sensors to capture pulse waves as measurable electrical signals.

Piezoelectric pulse sensors. Piezoelectric materials, which can be organic or inorganic, have the ability to sense dynamic pressure by converting mechanical force into electricity. In inorganic piezoelectric crystals, the piezoelectric effect is caused by the arrangement of ions within the symmetrical structure of the material[64–66], whereas in organic piezoelectric polymers, the piezoelectric effect is caused by the molecular structure and orientation of the polymer[67]. In the absence of an external force, randomly distributed or polarized dipoles have a net charge of zero. Conversely, when an external force is applied and deformation occurs, the piezoelectric effect causes these dipoles to reorient, resulting in a non-zero net charge[68] (Fig. 2).

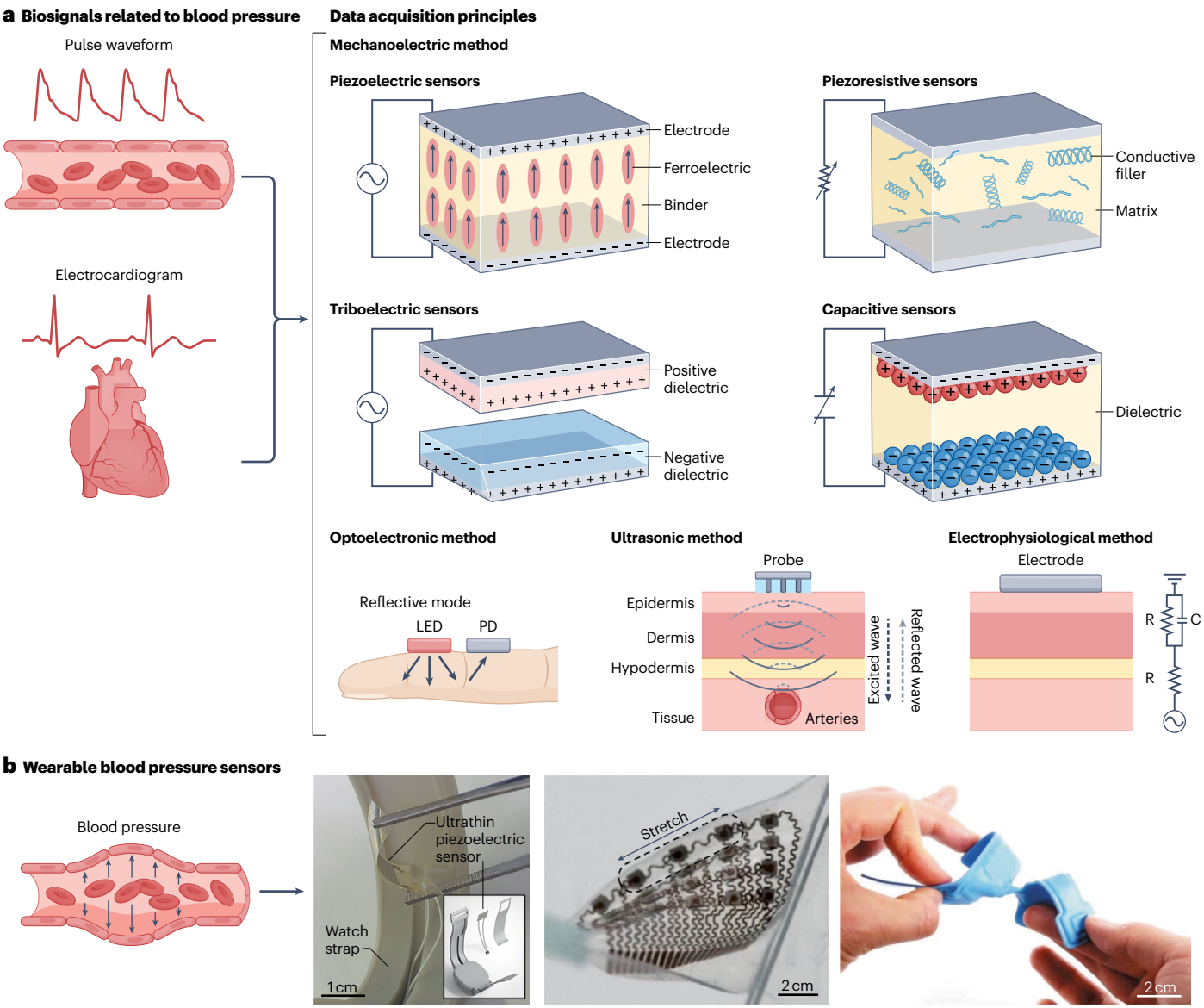

Fig. 1 | Wearable BP sensors for cardiovascular health care. a, Biosignals related to blood pressure (BP), including pulse waveforms and electrocardiographic data, are essential for monitoring cardiovascular health. Wearable BP sensors employ various data acquisition principles. Mechanoelectric methods detect mechanical pressure or deformation using piezoelectric, piezoresistive, triboelectric or capacitive sensors. Optoelectronic methods utilize photoplethysmography to optically measure changes in blood volume. Ultrasonic methods apply ultrasound technology to monitor arterial wall motion and blood flow. Electrophysiological methods measure electrical activities, such as electrocardiogram signals, to assess cardiac and vascular dynamics. These diverse approaches enable the precise capture of biosignals necessary for accurate BP estimation. **b**, Wearable BP sensors using various BP estimation methods. The three images on the right show flexible piezoelectric sensors based on pulse wave analysis, flexible ultrasound sensors that leverage arterial wall dynamics, and wearable limb sensors that employ pulse wave velocity assessment. C, capacitor; LED, light-emitting diode; PD, photodetector, R, resistor. Part **b** adapted with permission from ref. 237, John Wiley and Sons; adapted from ref. 141, Springer Nature; and adapted from ref. 175, Springer Nature.

The past 10 years have seen the development of new materials and composites for piezoelectric pulse sensors that improve their performance and applicability for wearable health monitors. Inorganic piezoelectric materials, such as lead zirconate titanate (PZT) and barium titanate (BTO) typically have large piezoelectric constants, making them highly sensitive to mechanical stress[69]. However, these materials are brittle and often contain harmful substances such as lead, limiting their use in biosignal measurement. To address these issues, researchers have developed ultrathin films[53] and nanocomposites[22] of these inorganic materials. These ultrathin structures maintain high sensitivity while increasing flexibility and reducing brittleness. For example, PZT thin films have been successfully transferred onto flexible substrates that are highly sensitive and mechanically stable. These thin films are fabricated using techniques such as the laser lift-off process,

Table 1 | Biosignal acquisition principles

Principle	Sensing mechanism	Materials	Fabrication methods	Research direction
Mechanoelectric	Piezoelectric: materials generate an electric charge in response to mechanical stress	PVDF–TrFE[71], BTO–PVDF[22] and PZT[53,58,171,237]	Spin-coating (laser lift-off)[53,237], mechanical thinning[171] and electrospinning[72]	Improvements in flexibility and sensitivity to enhance skin conformity and performance in wearable applications
	Triboelectric: electric charge generated through the contact and separation of two different materials	PDMS[81], nylon[78,81], PEDOT–PSS[83], PTFE[78,80,87] and Kapton[88]	Spin-coating[83], screen-printing[82], weaving[89], reactive ion etching[76,80,87,88] and self-assembly[78]	Development of textile-based sensors with conductive nanomaterial coatings to improve sensitivity and durability
	Piezoresistive: changes in electrical resistance in response to mechanical strain	PDMS–rGO[96], MXene[90,93], PANI–PDMS[98], rGO–PU[97] and PUA[94]	Solution dip-coating[90,96,97], bidirectional prestretch reaction[93], spin-coating[98] and micromoulding[94]	Improvement in sensitivity through the use of micropatterned and porous dielectric materials
	Capacitive: changes in electrical capacitance when a dielectric material is deformed	PDMS[43,104–106,108] (with CNT, AgNW and ITO), PVDF or IL[113], and PVA or phosphoric acid[114]	Microfluidic-assisted emulsion self-assembly[108], spin-coating[43], moulding[104–106,114] and immersing[113]	Development of microscale and nanoscale sensor architectures and iontronics to improve sensitivity
Photoplethysmography	Light-based technology to detect blood volume changes in the microvascular bed of tissue	TFB[121], F8BT[121], TBT[121], TCTA–Ir(ppy)$_3$[119] and NPB–Ir(MDQ)$_2$acac–B3PYMPM[119]	Blade coating[121], spin coating[121,122] and thermal evaporation[119]	Development of organic-based LED and signal processing techniques to minimize external noise and motion-related distortions
Ultrasonic	Utilizes high-frequency sound waves for various diagnostic purposes, measuring the frequency shift of reflected waves in Doppler mode to determine tissue motion and blood flow	PZT (1–3 composite)[99,142,143,146]	Multilayered microfabrication[142], welding[141] and dicing[144]	Development of flexible or stretchable arrays of ultrasonic transducers for advanced imaging and efficient power sources for the integration of compact devices
Electrophysiology	Measurement of electrical activity of the heart through skin contact	Liquid metal[159] and CNT or AgNW[160]	Electrospinning[159], spray coating[160] and molding[160]	Development of dry electrode materials to improve signal quality and user comfort

AgNW, silver nanowire; B3PYMPM, 4,6-bis(3,5-di(pyridin-3-yl)phenyl)-2-methylpyrimidine; BTO, barium titanate; CNT, carbon nanotube; F8BT, poly((9,9-dioctylfluorene-2,7-diyl)-*alt*-(2,1,3-benzothiadiazole-4,8-diyl)); IL, 1-butyl-3-methylimidazolium hexafluorophosphate; Ir(MDQ)$_2$acac, bis(2-methyldibenzo[f,h]quinoxaline); Ir(ppy)$_3$, tris[2-phenylpyridinato-C2,N]; ITO, indium tin oxide; LED, light-emitting diode; NPB, *N*,*N*′-di(1-naphthyl)-*N*,*N*′-diphenyl benzidine; PANI, polyaniline; PDMS, polydimethylsiloxane; PEDOT, poly(3,4-ethylenedioxythiophene); PSS, poly(styrenesulfonate); PTFE, polytetrafluoroethylene; PVA, polyvinyl alcohol; PVDF, polyvinylidene fluoride; PZT, lead zirconate titanate; PU, polyurethane; PUA, polyurethane acrylate; rGo, reduced graphene oxide; TBT, poly((9,9-dioctylfluorene-2,7-diyl)-*alt*-(4,7-bis(3-hexylthiophene-5-yl)-2,1,3-benzothiadiazole)-2′,2′-diyl); TCTA, tris(4-carbazoyl-9-ylphenyl) amine; TFB, poly(9,9-dioctylfluorene-*co*-n-(4-butylphenyl)-diphenylamine); TrFE, trifluoroethylene.

which involves the transfer of high quality piezoelectric thin films onto ultrathin plastic substrates[53]. In addition, the encapsulation of thin film PZT sensors in a polymethylsiloxane (PDMS) layer improved longevity and stability for continuous health-monitoring applications. Furthermore, PZT nanocomposites utilize a nanocomposite matrix of PZT nanoparticles dispersed in a PDMS matrix, functionalized with 3-glycidoxypropyltrimethoxysilane and the non-ionic surfactant Triton X-100 to enhance nanoparticle dispersion and reduce aggregation[22]. This composite structure has been shown to improve the uniformity and stability of the sensor, facilitating reliable pulse wave monitoring without the issues of aggregation and precipitation that are found in less advanced composites. In addition, these nanocomposites have been engineered to improve vapour permeability, which is crucial for long-term skin attachment and reducing skin irritation[70].

The development of lead-free piezoelectric materials is a crucial area of research due to health and environmental concerns associated with lead-based materials. Polyvinylidene fluoride (PVDF) and its copolymers have emerged as promising alternatives to lead-based materials[71]. Although these polymers show lower piezoelectric coefficients than their lead-based counterparts, they offer substantial advantages in terms of flexibility and biocompatibility. Innovations in polymer processing techniques, such as electrospinning, have facilitated the development of PVDF nanofibres with improved piezoelectric responses by increasing their surface area and achieving aligned molecular structures[71].

Hybrid materials that combine the benefits of inorganic and organic components are also promising. For example, the incorporation of inorganic nanoparticles, such as BTO or zinc oxide, into a PVDF matrix can improve the piezoelectric response while maintaining flexibility and biocompatibility[22,72]. A notable development in this area is the creation of hierarchical composites, whereby the piezoelectric nanoparticles are distributed in a controlled manner within the polymer matrix to optimize the overall performance of the material[73].

Triboelectric pulse sensors. Triboelectric effects occur when two dissimilar materials come into close contact, generating electricity through electron transfer between their overlapping electron clouds[74,75]. This process involves two stages: contact and separation. In the contact state, the materials neutralize their opposite charges, resulting in no current flow. In the separation state, the materials

become either negatively or positively charged, creating a current flow due to the electron potential difference (Fig. 2a).

Triboelectric sensors for pulse-to-electricity conversion benefit from structural simplicity, customizable biocompatibility, and being lightweight and low cost. Advances that have allowed the integration of nanostructured materials have led to increases in surface area and improvements in the triboelectric effect[76–79]. Furthermore, the incorporation of nanograted surfaces on triboelectric layers has also improved the charge density and output performance of the sensors. These nanostructures provide a larger contact area at the microscopic level to increase electron transfer and overall sensitivity.

In addition to nanostructuring, advances in material design strategies have been crucial in improving triboelectric pulse sensors. Structures inspired by kirigami, the Japanese art of cutting and folding paper, have been introduced to improve sensor flexibility and adaptability to human skin[80]. Embedding functional intermediate layers into the friction layer can improve inductive charge, electrical output and charge retention by using high dielectric materials, or by adding charge storage, electron blocking and electron transmission layers[81,82]. High dielectric constant electron blocking layers can improve polarization, whereas multilayer structures with electron trapping layers made from materials, such as PDMS, can improve output by trapping and transferring electrons more efficiently[81]. Advances in interlayer materials, such as multifunctional layered graphene and composites of multiwalled carbon nanotube with PVDF copolymerized with trifluoroethylene, have increased triboelectric performance compared with devices without interlayers or those using conventional single material interlayers[82]. Organic polymers, with their chemical and physical electron trapping sites, can further enhance triboelectric performance[83,84].

The development of textile-based triboelectric sensors is another major advance in material science. By embedding conductive fibres or yarns into fabrics, researchers have created wearable sensors that maintain breathability, tactility and mechanical robustness, with improved sensitivity due to surface roughness[85]. These textiles are typically made from synthetic fibres coated with nanomaterials to boost their triboelectric properties[86–88]. For example, a machine-knitted washable sensor array textile that has high pressure sensitivity and durability has been developed for precise epidermal physiological signal monitoring[89]. Importantly, the textile form allows easy integration into clothing to facilitate unobtrusive health monitoring.

Piezoresistive pulse sensors. Piezoresistive sensors convert applied pressure on their surface into a change in resistance through the piezoresistive effect, thereby generating an electrical signal for pressure measurement and monitoring[90,91] (Fig. 2a). Advances in piezoresistive pulse sensors over the past 10 years have focused on the development of materials and structures that can improve their sensitivity and flexibility, including the use of micropatterned structures. By employing lithography or template methods, researchers have created microsized or nanosized designs, such as pyramids[92,93], pillars[94], hollow spheres[95], porous structures[90,96,97] and wrinkles[98], in the dielectric layer. These patterns substantially increase the sensor's surface area, resulting in greater sensitivity to pressure changes due to the large surface area changes induced by small forces.

The integration of advanced composite materials has also had a crucial role in the development of piezoresistive sensors. The combination of materials, such as MXene[90,93] and graphene[97,99], known for their high conductivity and mechanical strength, with flexible substrates can lead to the generation of highly sensitive and durable sensors. Fabric-based piezoresistive sensors are gaining attention for their potential in wearable applications[100–102]. By integrating conductive fibres or yarns into textiles, researchers have created sensors that are both breathable and mechanically robust. These textiles can detect pulse waves with high sensitivity due to the increased surface roughness and the inherent flexibility of the fabric.

Capacitive pulse sensors. A capacitive sensor, consisting of top and bottom electrodes, an insulator and a substrate, alters its capacitance when pressure is applied perpendicularly, as the deformation of the film changes the distance between the electrodes (Fig. 2a). This change is governed by the relationship in which the capacitance depends on the space permittivity, the relative permittivity of the dielectric material, the overlapping area of the electrodes and the separation between the electrodes[56]. Typically, capacitive sensors use a parallel plate design, in which any changes in the overlapping area and the separation due to applied force result in non-linear capacitance variations[103]. These sensors are valued for their simple design and production, but have limitations, such as small capacitance variations and reduced sensitivity with smaller sizes.

Various design strategies have been employed to improve the performance of the material. Micropatterned structures, such as micropyramids, micropillars and microhemispheres, have been

Table 2 | Comparative analysis of sensing principles in wearable BP sensors

Principle	Advantages	Disadvantages
Mechanoelectric: piezoelectric	Low power consumption (self-powered); wide range of frequency response; high sensitivity	Limited dynamic pressure; high impedance
Mechanoelectric: triboelectric	Low power consumption (self-powered); cost-effective; high sensitivity	Limited dynamic pressure; durability issues; noise sensitivity
Mechanoelectric: piezoresistive	Dynamic and static measurement; simple methodology	High power consumption; sensitive to temperature
Mechanoelectric: capacitive	Dynamic and static measurement	Sensitive to humidity and temperature; small capacitance variation
Photoplethysmography	Simple methodology; cost-effective	Influenced by ambient light and skin tone; high power consumption; sensitivity to noise
Ultrasonic	High depth penetration; high resolution	Complex signal processing; high power consumption; high cost
Electrophysiology	Accurate heart activity monitoring; direct measurement; high temporal resolution	Complex signal processing; limited utility for direct blood pressure estimation

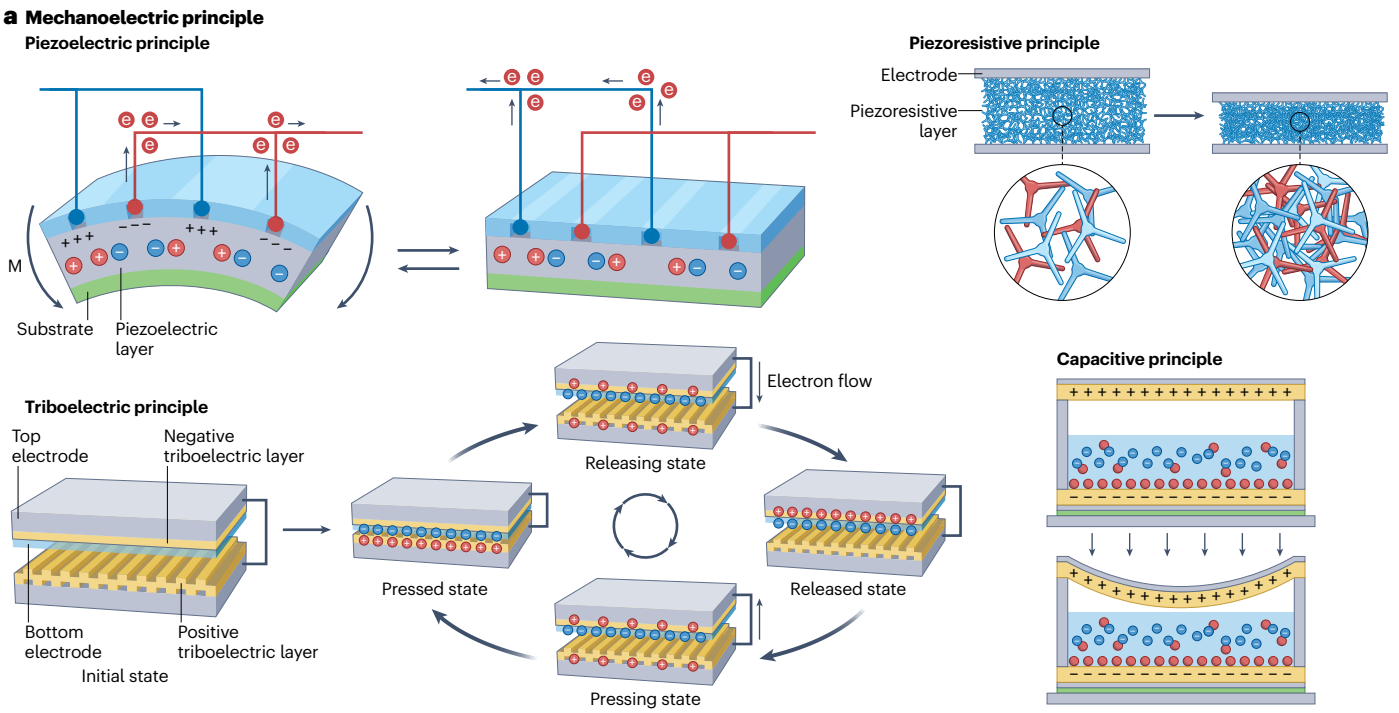
a Mechanoelectric principle
Piezoelectric principle
M
Substrate
Piezoelectric layer
Piezoresistive principle
Electrode
Piezoresistive layer
Triboelectric principle
Top electrode
Negative triboelectric layer
Bottom electrode
Positive triboelectric layer
Initial state
Pressed state
Releasing state
Electron flow
Released state
Pressing state
Capacitive principle

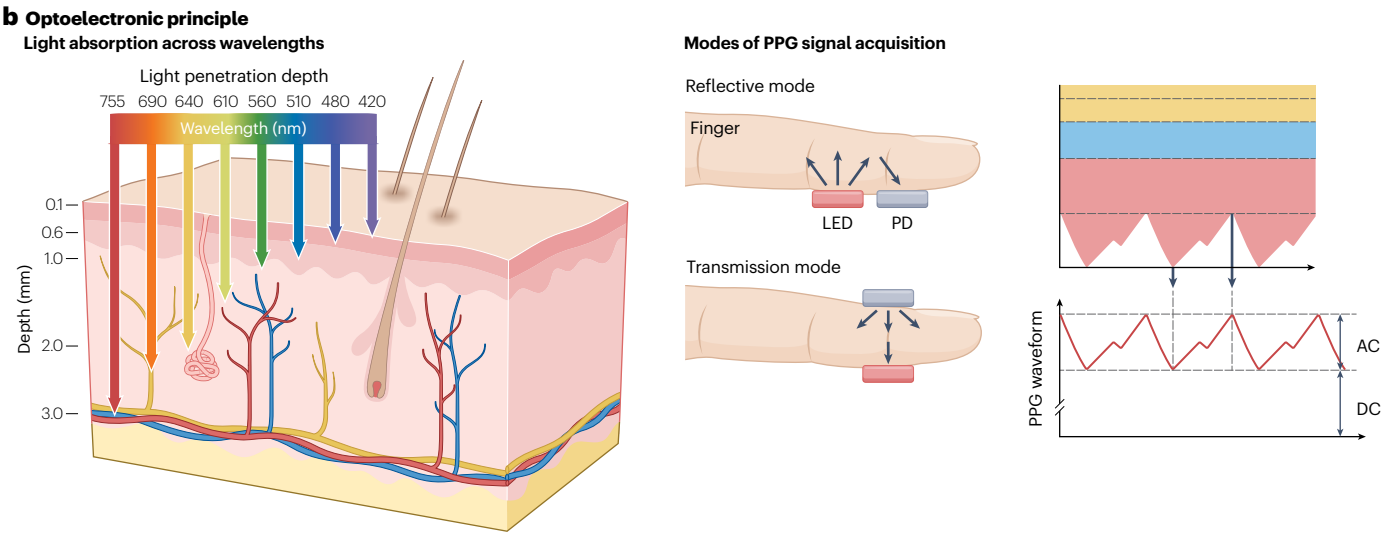
b Optoelectronic principle
Light absorption across wavelengths
Light penetration depth
755 690 640 610 560 510 480 420
Wavelength (nm)
Depth (mm)
0.1
0.6
1.0
2.0
3.0
Modes of PPG signal acquisition
Reflective mode
Finger
LED
PD
Transmission mode
PPG waveform
AC
DC

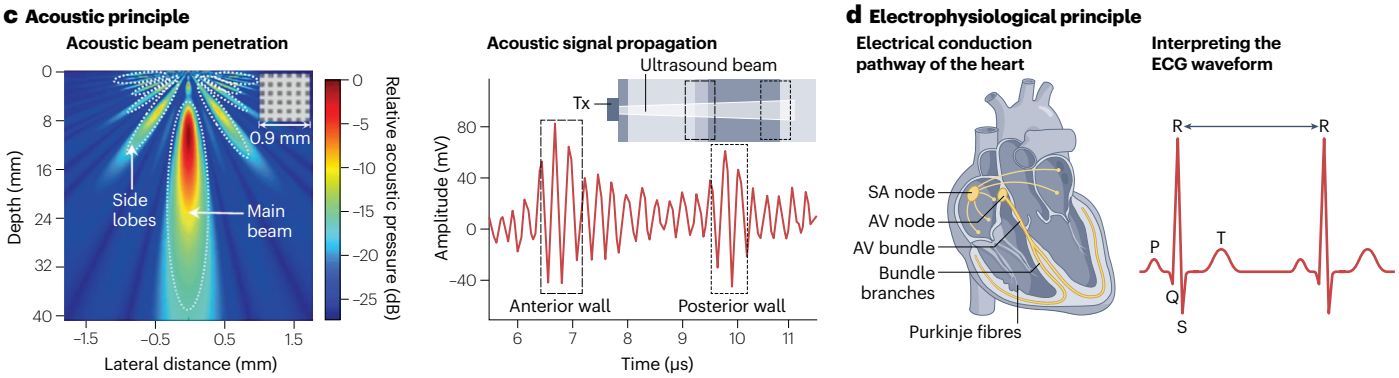
c Acoustic principle
Acoustic beam penetration
Depth (mm)
0
8
16
24
32
40
0.9 mm
Side lobes
Main beam
-1.5
-0.5
0.5
1.5
Lateral distance (mm)
Relative acoustic pressure (dB)
0
-5
-10
-15
-20
-25
Acoustic signal propagation
Ultrasound beam
Tx
Amplitude (mV)
80
40
0
-40
Anterior wall
Posterior wall
6
7
8
9
10
11
Time (μs)
d Electrophysiological principle
Electrical conduction pathway of the heart
SA node
AV node
AV bundle
Bundle branches
Purkinje fibres
Interpreting the ECG waveform
R
R
P
T
Q
S

Fig. 2 | Principles of biosignal data acquisition related to BP. **a**, Mechanoelectric principle for pressure sensors. Piezoelectric sensors convert mechanical stress into electrical signals through the piezoelectric effect. These sensors use piezoelectric materials that generate voltage when deformed, enabling detection of pressure changes. Triboelectric sensors operate by transferring charge when two materials make contact and separate, producing signals correlated with pressure variations. Piezoresistive sensors detect changes in electrical resistance caused by the deformation of a conductive material under pressure, providing pressure data. Capacitive sensors function by measuring changes in capacitance between two electrodes separated by a dielectric layer, with deformation altering capacitance to reflect pressure changes. **b**, Optoelectronic principles for photoplethysmography (PPG) sensors. The illustration on the left portrays light with different wavelengths penetrating tissues, emphasizing the importance of selecting suitable wavelengths for accurate biosignal acquisition. The panel on the right depicts the placement of a light-emitting diode (LED) and photodetector (PD) for reflective and transmission modes. The PPG signal consists of direct current (DC) and alternating current (AC) components, representing baseline tissue light absorption and changes in blood volume due to pulsatile flow. **c**, Acoustic principle for ultrasonic sensor. Ultrasonic sensors utilize piezoelectric materials to emit high-frequency sound waves, generating an acoustic profile for imaging arteries (left panel). Received ultrasound echoes from the anterior and posterior vessel walls of the ulnar artery, used to measure arterial dimensions (right panel). **d**, Electrophysiological principle for electrocardiogram (ECG) sensors. The left panel depicts the electrical conduction process in the heart, which drives cardiac cycles. The right depicts an ECG recording of electrical activity, including P waves, QRS complexes and T waves, used for cardiovascular monitoring. M, mechanical stress; AV, atrioventricular; SA, sinoatrial; Tx, transducer. Part **a** adapted with permission from ref. 68, John Wiley and Sons; adapted with permission from ref. 76, Elsevier; adapted with permission from ref. 90, Elsevier; and adapted from ref. 103, CC BY 4.0 (https://creativecommons.org/licenses/by/4.0/). Part **b** adapted from ref. 60, CC BY 3.0 (https://creativecommons.org/licenses/by/3.0/). Part **c** adapted from ref. 141, Springer Nature.

shown to increase sensitivity when integrated into dielectric layers due to increased surface area[104–107]. Porous microstructures introduce additional air voids, further increasing sensitivity by allowing greater deformation under pressure[43,108,109]. The main advantage of porous layers is the increased compressibility of the dielectric layer due to the incorporation of air voids, which have a lower dielectric constant and do not resist deformation. Elastomers, foams and sponges, such as PDMS and silicone-based elastomers, are often structured as porous or sponge-like dielectrics and offer high compressibility and recoverability. Wrinkled dielectric materials, such as silver nanowires embedded in PDMS, can increase sensitivity through increased deformation under pressure[110,111]. However, sensitivity remains limited by the pressure measurement range due to low compressibility, which decreases the reliability of sensors and electronic skins after repeated loading and unloading cycles. To address this issue, several research groups have explored the use of ionic fluids and iontronics[112]. Fluidic and ionic liquids, such as those used in iontronic materials, serve as dielectrics to increase flexibility, signal intensity and sensitivity by leveraging electric double layer capacitance[113,114].

Optoelectronic principles

PPG is a promising non-invasive method for cardiovascular monitoring by determining volumetric changes in circulating blood through variations in light intensity caused by the pulsatile movement of blood vessels. Optoelectronic devices, such as light emitters and photodetectors, have been integrated with PPG devices to transduce light into blood vessels and detect scattered photo signals. For effective light delivery, light-emitter materials are typically selected within the red and near-infrared wavelength ranges, which allows penetration to 2–3 mm below the skin surface[115] (Fig. 2b, left panel). Additionally, green light has been found to be highly effective for measuring superficial blood flow due to its strong absorption by haemoglobin, providing a better signal-to-noise ratio than infrared light[116]. As a result, green light-emitting diodes (LEDs) are increasingly used in commercial PPG devices for their high accuracy and reliability in detecting pulse rates.

The scattered photo signals are obtained from photodetectors using either the transmission or reflection measurement principle (Fig. 2b, central panel). In transmission mode, photodetectors are located opposite the light sources, providing clear signals but limiting the detection area to the fingertips, cheeks or nasal septum where incident photons can enter the photodetectors[60]. By contrast, reflection mode allows measurements in more body regions by arranging light sources and photodetectors in parallel, although signal reliability is substantially affected by motion artefacts and pressure disturbances.

The PPG waveform can be divided into two components: direct current and alternating current. The direct current element contains information acquired from reflected or transmitted light that varies with tissue structure, blood volume and respiration rate. The alternating current element depicts fluctuations in blood volume that occur between the systolic and diastolic phases of the cardiac cycle. These components provide a comprehensive overview of cardiovascular function and are crucial for accurate interpretation of PPG signals[60] (Fig. 2b, right panel).

PPG sensors have several advantages compared with mechanoelectric sensors that make them particularly useful for non-invasive cardiovascular monitoring. One of the primary benefits is their simplicity and cost-effectiveness, given that they use readily available optoelectronic components, such as LEDs and photodetectors. PPG sensors can measure various cardiovascular parameters, including heart rate, heart rate variability, blood oxygen saturation, respiration rate and BP via advanced algorithms and signal processing techniques[24,116–118].

Over the past decade, optoelectronic devices, such as flexible organic LEDs[119–121], polymer LEDs[122–124] and organic–inorganic hybrid devices[125], have contributed to improved mechanical durability and sensitivity of PPG sensors. Organic materials, valued for their flexibility, lightweight nature and cost-effective fabrication methods, have been utilized to create skin-compatible sensors that maintain high performance under mechanical deformation. Organic–inorganic hybrid devices combine the flexibility and lightweight nature of organic materials with the superior electronic properties of inorganic components, such as high charge mobility, stability and efficient light absorption. This synergy results in devices with enhanced mechanical robustness, high sensitivity and improved operational efficiency, making them ideal for applications requiring both performance and adaptability, such as wearable sensors[125]. These advances hold great potential for more reliable and efficient wearable health monitoring solutions.

Despite these advantages, the accuracy of PPG sensors is limited by their susceptibility to motion artefacts[126,127], by variations in skin tone and thickness[128,129] and by environmental interference from ambient light[130] and temperature[131]. To address these limitations, researchers

have developed advanced algorithms and signal processing techniques to filter out artefacts[126,132,133]. Furthermore, they have assessed adaptive calibration and multiwavelength approaches[134], and have tested the feasibility of combining PPG with other sensing modalities, such as accelerometers[135] and piezoelectric transducers[136], to improve accuracy and reliability.

Ultrasonic principles

Ultrasound waves can penetrate deeply into biological tissues to allow non-invasive acquisition of numerous cardiovascular parameters. Ultrasonic sensors detect deep-tissue signals by measuring the reflection or attenuation of incident waves upon transmission into the deep skin that is caused by acoustic impedance differences between tissue layers. These reflected signals contain embedded anatomical and physiological information[137–140].

Transducers are used to transmit ultrasound waves into the human body and receive the reflected echoes. The number of transducers determines the penetration depth of the ultrasound waves, which focuses the beam intensity. A single transducer allows a penetration depth of up to 40 mm under the skin[141] (Fig. 2c, left panel), whereas ultrasound waves from a transducer array allow a penetration depth of up to 164 mm[142]. During wave propagation into vessels, acoustic echoes are generated at the anterior and posterior walls by reflection (Fig. 2c, right panel). These echoes facilitate the precise identification of the position, dimensions, morphology and structure of vessels, allowing the measurement of BP waveforms by detecting changes in vessel diameter over time[141]. In addition, ultrasound sensors provide high resolution images of deep tissue structures, making them ideal for measuring numerous functional cardiac parameters, such as stroke volume and cardiac output[141,143,144]. Traditional ultrasound probes require skilled operators, thus limiting their usage to clinical settings. However, the development of flexible and stretchable ultrasonic transducers opens up their potential applicability for wearable technologies, enabling continuous, operator-independent monitoring.

One of the key breakthroughs in wearable ultrasound technology is the development of stretchable ultrasonic transducers using materials such as PDMS and one to three piezoelectric composites[137,141,145,146]. These materials provide low acoustic impedance, which closely matches that in human tissues, allowing better signal transmission and reception. The incorporation of epoxy resins and PDMS between piezoceramic elements increases the flexibility of the composites, enabling them to conform to various body shapes and maintain consistent contact with the skin during movement. Furthermore, styrene–ethylene–butylene–styrene (SEBS) has been integrated into transducers to improve their performance. SEBS provides exceptional elasticity and durability, ensuring that the transducers can withstand repeated stretching and bending without compromising their functionality[143]. In addition, the solvent soldering process using SEBS-based materials facilitates the secure attachment of the piezoelectric elements to the substrate, allowing the maintenance of robust electrical connections even under mechanical stress.

Electrophysiological principles

The heart generates electrical signals at the sinoatrial node, which subsequently propagates across the cardiac conduction system. This system includes the atrioventricular node, the atrioventricular bundle, the right and left bundle branches, and the Purkinje fibres[147–149] (Fig. 2d, left panel). An ECG records the differences in electrical potential produced by heart activity, providing information on heart rhythm and rate. The ECG waveform consists of the P wave (atrial depolarization), the QRS complex (ventricular depolarization) and the T wave (ventricular repolarization). Another important parameter is the R-R interval, which denotes the time between successive R waves, and is used to estimate heart rate[150–153] (Fig. 2d, right panel).

During an ECG recording, electrodes attached to the skin detect electrophysiological changes caused by the depolarization and repolarization of heart muscles. Three types of electrodes have been assessed: wet, dry and non-contact electrodes[154]. Wet electrodes, which consist of an electrolyte gel, provide clear signal quality by improving conformal contact with human skin and minimizing air gaps. Although silver-based or silver chloride-based wet electrodes are most commonly used as reference electrodes, hydrogels are promising materials for wet electrodes because they have similar mechanical properties to human tissue[155]. Wet electrodes are limited by short usage time, given that the gel tends to dry out over time. To address this issue, dry electrodes that do not require electrolyte solution or gel have been developed[156–160]. Dry electrodes are made from metal or conductive polymers, with soft conductive polymers preferred for better skin adhesion[161]. Non-contact electrodes, which do not directly contact the skin, offer advantages such as reusability, minimal motion artefacts and reduced risk of electrical issues, irritation or allergic reactions[162]. Non-contact electrodes with elastic dielectric layers can further reduce motion artefacts. Silicone-insulated gold electrodes are less sensitive to body motion than wet electrodes, but still maintain capacitive coupling with the skin, as shown by clearer ECG signals compared with conventional gel electrodes[163].

BP estimation theories

The cuff-based oscillometric strategy to measure BP was historically used owing to its high accuracy[164]. This method measures three types of BP: systolic BP (SBP; the maximum pressure during heart contraction), diastolic BP (DBP; the maximum pressure during heart relaxation) and mean arterial pressure (the average pressure during one cardiac cycle and a major indicator of organ perfusion). However, the need for repeated cuff inflation and deflation limits the use of oscillometric devices to measuring only intermittent BP readings, and not for continuous monitoring. To overcome this issue, alternative approaches such as PWA, PWV and arterial wall dynamics have been adopted, using measurements derived from PPG devices, ECG and ultrasonography. These approaches allow continuous, non-invasive BP monitoring and real-time cardiovascular health tracking.

Although these strategies are promising, the measurement of single peripheral waveforms alone might make it difficult to differentiate between changes in stroke volume and peripheral resistance, leading to inaccuracies in BP estimation. Single peripheral waveforms can change due to various cardiovascular factors and are usually coupled with alternating currents, but measuring constant pressure levels requires coupling with direct currents, which peripheral waveforms typically do not provide[165]. Nonetheless, emerging studies continue to show correlations between single peripheral waveforms measured from peripheral arteries and key cardiovascular indicators, such as BP and variations in stroke volume[166–168]. As a result, advances in sensor materials, coupled with improvements in signal processing and calibration technologies, will help to overcome these limitations.

PWA theory

PWA assesses the characteristics of arterial pulse waveforms to estimate cardiac output and other haemodynamic variables, such as augmentation index and BP. This technique analyses two distinct waves within

the arterial pulse: the initial forward wave, generated by ventricular contraction, and the reflected wave, which originates from the peripheral circulation and travels back towards the heart. PWA focuses on specific features of these waves, such as the timing and amplitude of systolic and diastolic peaks, which are highly correlated with BP and are used to estimate BP through linear regression[169] (Fig. 3a, left panel). ML algorithms have also been used to improve the accuracy of BP estimation by considering a broader range of features and patterns within the pulse waveform[170]. One important advantage of PWA over other modalities is that it can potentially allow accurate BP estimation using just a single sensor, increasing portability and ease of use.

In addition, studies in PWA have established correlations between piezoelectric pulse waves and BP waves to further refine BP estimation methods (Fig. 3a, right panel). Piezoelectric arterial pulse wave dynamics are traditionally considered similar to typical BP waves. However, achieving accurate continuous BP monitoring on the basis of arterial pulse waves remains challenging owing to unclear correlations between piezoelectric pulse waves and BP waves. Although piezoelectric pulse waves resemble typical BP waves, the exact relationship between the two remains unclear owing to the complex nature of how these waves interact with arterial dynamics. To address this issue, the correlation between piezoelectric pulse waves and BP waves has been elucidated through theoretical, simulation and experimental analysis[171].

PWV theory

PWV refers to the speed at which the pressure wave propagates along the circulatory system[85], and serves as an indicator of arterial stiffness. An increase in PWV implies progressive stiffening and reduced elasticity of blood vessels, and has been associated with cardiovascular conditions, such as hypertension and atherosclerosis[172]. PWV is determined by recording pulse waves at two sites, then dividing the distance between the measuring points by the time it takes for the pulse wave to travel between them[173–175]. Depending on the measurement location, the time differences of pulse waves are classified into two categories: pulse arrival time[176–178] and pulse transit time[178–182]. Pulse arrival time depicts the time it takes for a pulse wave to travel from the heart to a peripheral site, whereas pulse transit time depicts the time it takes for a pulse wave to travel between two arterial locations[183] (Fig. 3b). These values are utilized as independent variables to establish a relationship with BP estimation.

One of the distinctive advantages of PWV over PWA is its ability to provide additional information on cardiovascular parameters beyond BP. PWV can help measure the risk of atherosclerosis and arterial stiffness, as well as overall cardiovascular risk. By assessing the speed of pressure waves through the arteries, PWV gives a clearer picture of arterial health than PWA, making it useful for the early diagnosis and management of cardiovascular diseases[184,185].

Arterial wall dynamics theory

Wearable ultrasound sensors have enabled intuitive BP prediction by analysing real-time images of vein dynamics, particularly changes in blood vessel diameter (Fig. 3c). The time-dependent variations in vessel diameter correlate with BP using the following equation:

$$p(t) = p_{\mathrm{d}} \times e^{\alpha\left(\frac{A(t)}{A_{\mathrm{d}}}-1\right)}$$

In this equation, p_{d} is the diastolic pressure, $A(t)$ is the arterial cross-section at any given moment, A_{d} is the diastolic arterial cross-section and α is the vessel rigidity coefficient[141]. Assuming that the artery is rotationally symmetrical, $A(t)$ can be approximated as

$$A(t) = \frac{\pi d^2(t)}{4}$$

where by $d(t)$ is the diameter waveform of the target artery.

On the basis of this theory, central BP monitoring technology was introduced using wearable ultrasound sensors made with one to three piezoelectric composites as soft structural components. These sensors can continuously and accurately monitor BP from various body locations, such as the carotid, brachial, radial and pedal arteries, by measuring vessel diameter changes using the equation above[141]. Additionally, an epidermal patch with customized PZT ultrasound sensor transducers has been developed to track the carotid artery walls and calculate arterial BP waveforms based on vessel distension. This patch reliably measures BP during physical activity and has been validated against commercial cuff BP monitors[144].

Compared with PWA and PWV methods, the ultrasound approach offers several advantages. Ultrasound sensors can directly measure changes in arterial diameter to provide more accurate and immediate insights into BP variations. Whereas PWA and PWV rely on indirect assessments and are susceptible to motion artefacts and signal noise, the ultrasound approach is more precise and reliable, particularly during physical activity[141].

ML algorithms for BP estimation

ML techniques for measuring BP, renowned for their data-driven nature, have substantially improved the accuracy of BP estimation by adeptly interpreting distinct waveform patterns present in biosignals[186–192]. These techniques analyse biosignals to identify features crucial for BP estimation, such as time domain characteristics, ECG peaks and markers indicative of systolic and diastolic phases. This approach highlights the complex biological factors that work together to influence BP, and captures both linear and non-linear relationships inherent in the data. However, models that do not incorporate pulse waveforms often struggle to accurately estimate BP, particularly in individuals with high variability, such as during physical activity or stress. Baseline models that rely solely on calibration values or other parameters might perform adequately in certain subgroups, such as in younger or normotensive individuals, but they might not be as accurate in capturing the physiological changes that occur in other populations, such as in older individuals or those with hypertension and comorbidities[193]. Models that include pulse waveform data are better suited for extracting accurate signals that reflect dynamic changes, such as those induced by physical activity, stress or underlying cardiovascular conditions. This capability improves the robustness and adaptability of the model across a wider range of physiological states.

In general, ML methodologies for BP estimation can be categorized into two main subtypes: traditional ML and advanced deep learning (DL) approaches. Conventional ML techniques require meticulous manual extraction of features, a process that can be labour-intensive. By contrast, DL approaches eliminate the need for manual feature engineering due to its capability to autonomously learn intricate representations and relationships directly from raw data. This capability facilitates comprehensive end-to-end training for BP estimation, providing a unified and integrated methodology for estimating BP.

Traditional ML-based methods

Traditional ML-based algorithms depend on the utilization of information-rich features that require manual extraction and

meticulous engineering, making data preprocessing a pivotal step[194]. Key preprocessing tasks often involve signal de-noising to improve data quality[195,196], followed by normalization to ensure consistency across the dataset[194,197]. The extracted features are subsequently input into ML models, which aim to make predictions or estimations based on the processed feature input.

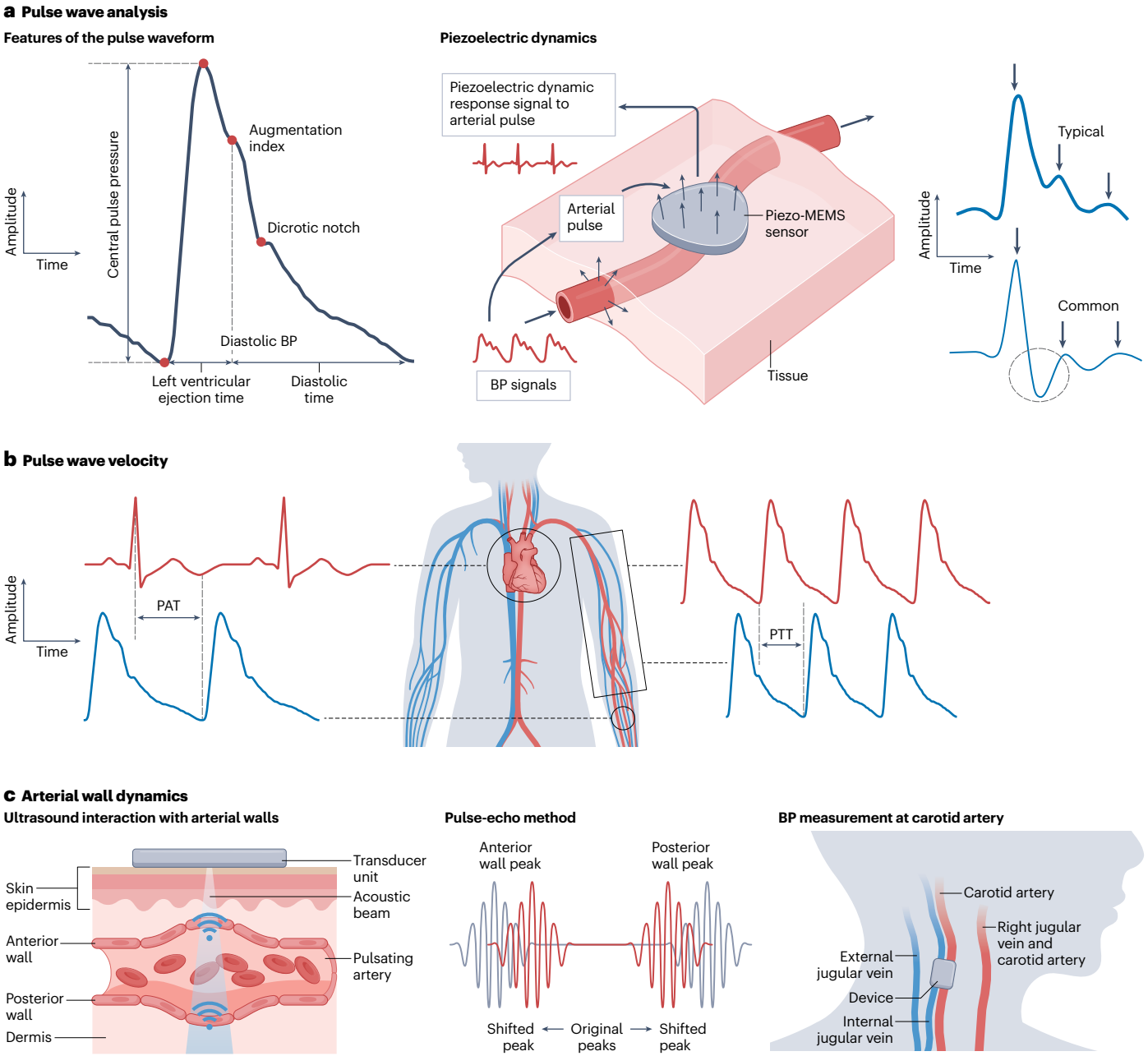

Fig. 3 | Biosignal analysis theories for BP estimation. a, Pulse wave analysis for blood pressure (BP) estimation. The left panel depicts the extraction of various feature points from radial pulse waveforms for pulse wave analysis. The right panel illustrates the piezoelectric dynamic response to arterial pulse using a piezo-MEMS sensor, which measures pulses by detecting mechanical deformations. The typical arterial pulse waveform shows an idealized pattern with three gradually weakening positive peaks, reflecting arterial pressure changes over time under optimal conditions and serving as a standard for analysing arterial pulse dynamics and BP estimation. By contrast, the common arterial pulse waveform features a strong reverse peak following the initial positive peak, representing real-world measurements often influenced by physiological variations, sensor placement or motion artefacts, highlighting the challenges of achieving consistent and artefact-free arterial pulse signals. **b**, Pulse wave velocity method for BP estimation. The difference between pulse arrival time (PAT) and pulse transit time (PTT) is shown. **c**, Arterial wall dynamics for BP estimation. The panel on the left depicts the principle underlying the recording of a pulsating blood vessel, which can be translated into localized BP waveforms. The middle and right panels depict the measurement of central BP on the human neck using an ultrasonic device. Ultrasound devices use a highly directed ultrasound beam to locate the dynamic anterior and posterior walls of blood vessels.

Linear regression is one of the most widely utilized ML algorithms for establishing the latent stochastic linear relationship between input variables and a target predictor. In BP estimation, physiological parameters such as pulse transit time, pulse arrival time and PWV are adopted with the assumption of a linear correlation with BP values[198]. Support vector machines are widely utilized in ML for tasks including regression, for which they aim to determine the optimal fitting line or hyperplane in multidimensional spaces that can minimize the discrepancy between predicted outcomes and actual data points within the feature space. For example, support vector machine regression has been applied to PPG signals, including those transformed using Shannon discrete wavelet, a method that decomposes signals into different frequency components while preserving their time information, allowing analysis of signals at multiple resolutions[186], as well as to features extracted from both PPG and ECG signals to estimate BP[199]. Random forest is an ensemble learning approach that generates a collection of decision trees during the training phase and aggregates their predictions using the mode for classification tasks or the average for regression tasks to increase predictive accuracy while mitigating the risk of overfitting. Random forest has been employed to explore the relationship between PPG signals, ECG signals and BP measurements[187].

Boosting is a ML technique that improves model accuracy by combining multiple weak learners, which are models that perform slightly better than random guessing. This method involves training a series of models sequentially, with each model focusing on correcting the errors made by the previous model. Adaptive boosting (also known as AdaBoost) iteratively adjusts the weights of misclassified instances, thus improving their subsequent classification[188]. This sequential approach ensures each learner focuses on correcting the mistakes of its predecessors. An AdaBoost multiclassifier has been applied to PPG signals, using it as an error correcting output coding technique[188]. Furthermore, other algorithms such as those based on *k*-nearest neighbours[200] and regression trees[201] have also been used for BP estimation.

DL-based methods

DL methods employ multilayered artificial neural networks that can autonomously learn from vast datasets, and thus excels in pattern recognition and comprehension beyond what shallow learning models can achieve. This proficiency has been demonstrated across various domains, including computer vision[202–207], natural language processing[208–211] and speech recognition[212–215], in which DL substantially outperforms traditional ML algorithms in handling complex analytical tasks[216,217].

The recurrent neural network (RNN) is a foremost DL algorithm for processing time series data[218,219], including biosignals such as BP[220,221]. This network is adept at retaining a memory of past input sequences within its hidden states, effectively capturing the underlying patterns of the data. A major challenge for RNNs is the vanishing gradient problem (whereby the gradients that are used to update the network become extremely small or 'vanish' as they are back-propagated from the output layers to the earlier layers), which impedes learning long-range dependencies. Long short-term memory (LSTM) networks, a prominent variant of RNNs, are specifically designed to overcome this limitation through an input-dependent gating mechanism. This advanced architecture enhances the model's ability to retain and utilize information from earlier inputs over extended periods, thereby improving its capability in processing and predicting outcomes from time-dependent data. A personalized LSTM network approach for continuous BP monitoring has been introduced, whereby features are directly learned from PPG signals within deep neural networks[189]. In addition, a calibration-free BP estimation method using a bidirectional LSTM (BiLSTM) network on ECG and PPG signals and a multilayer residual BiLSTM (Fig. 4a) network on PPG and ECG signals has also shown promising results in accurately predicting BP without the need for calibration[220,222].

The convolutional neural network (CNN), noted for its effectiveness in processing large-sized, multidimensional data, has also been utilized for BP estimation. By utilizing the locality property of convolutional kernels, CNNs excel at handling continuous data streams such as images[202–205] and speech[212,213,223], enabling precise and efficient feature extraction and analysis. Moreover, CNNs benefit from strong parallel computing capabilities, which substantially reduce both computational time and costs. Advanced variants such as dilated convolutions and temporal convolutional networks further enhance the utility of CNNs by improving their ability to capture causal and temporal information, thus supporting more effective time-dependent modelling. For example, CNNs have been used to directly generate latent features from PPG pulse waves, with the aim of facilitating a more continuous and streamlined BP estimation process[224–226]. Additionally, a deep CNN network that processes raw signals without the need for PWV feature extraction has been developed, allowing end-to-end BP estimation without calibration[190] (Fig. 4b).

The convolutional RNN, which integrates the strengths of CNN and RNN, has been used to analyse multidimensional time-series data. Its hybrid architecture design capitalizes on the local feature extraction capabilities of CNNs and the sequential data processing power of RNNs[227–229]. This synergy allows an efficient extraction and thorough analysis of hidden features within complex sequential data. For example, a CNN–LSTM model was implemented on the ECG–PPG difference signal, enabling simultaneous predictions of SBP and DBP from shared layers[191].

A new DL architecture, known as the transformer, utilizes an attention mechanism that adeptly discerns semantic correlations among sequence elements, substantially enhancing its ability to understand complex data[230]. This advanced capability enables transformer models to excel in tasks that demand a deep comprehension of intricate data and their interconnections, outperforming previous models across various domains, including computer vision[206,207], natural language processing[208–211] and generation, and speech recognition[214,215]. Despite its effectiveness, the main challenge with the transformer model is its high computational demand, which complicates deployment in resource-constrained environments, such as small wearable devices for local BP estimation. To address this issue, a transformer-based BP estimation model was proposed that incorporates knowledge distillation and transfer learning to facilitate efficient BP estimation with a lightweight architecture[192] (Fig. 4c).

Generative model-based methods

Although the methods described above focus on understanding the relationship between input data and corresponding output values to enable accurate classification and regression predictions, another category of ML known as generative models aims to understand the underlying distribution of data and to generate new samples from the estimated training data distribution[215]. Traditional generative ML models include Gaussian mixture models (GMM) and hidden Markov models (HMM), which are foundational techniques for modelling the distribution of data. GMMs represent data as a mixture of several Gaussian distributions, facilitating the parametric modelling of complex

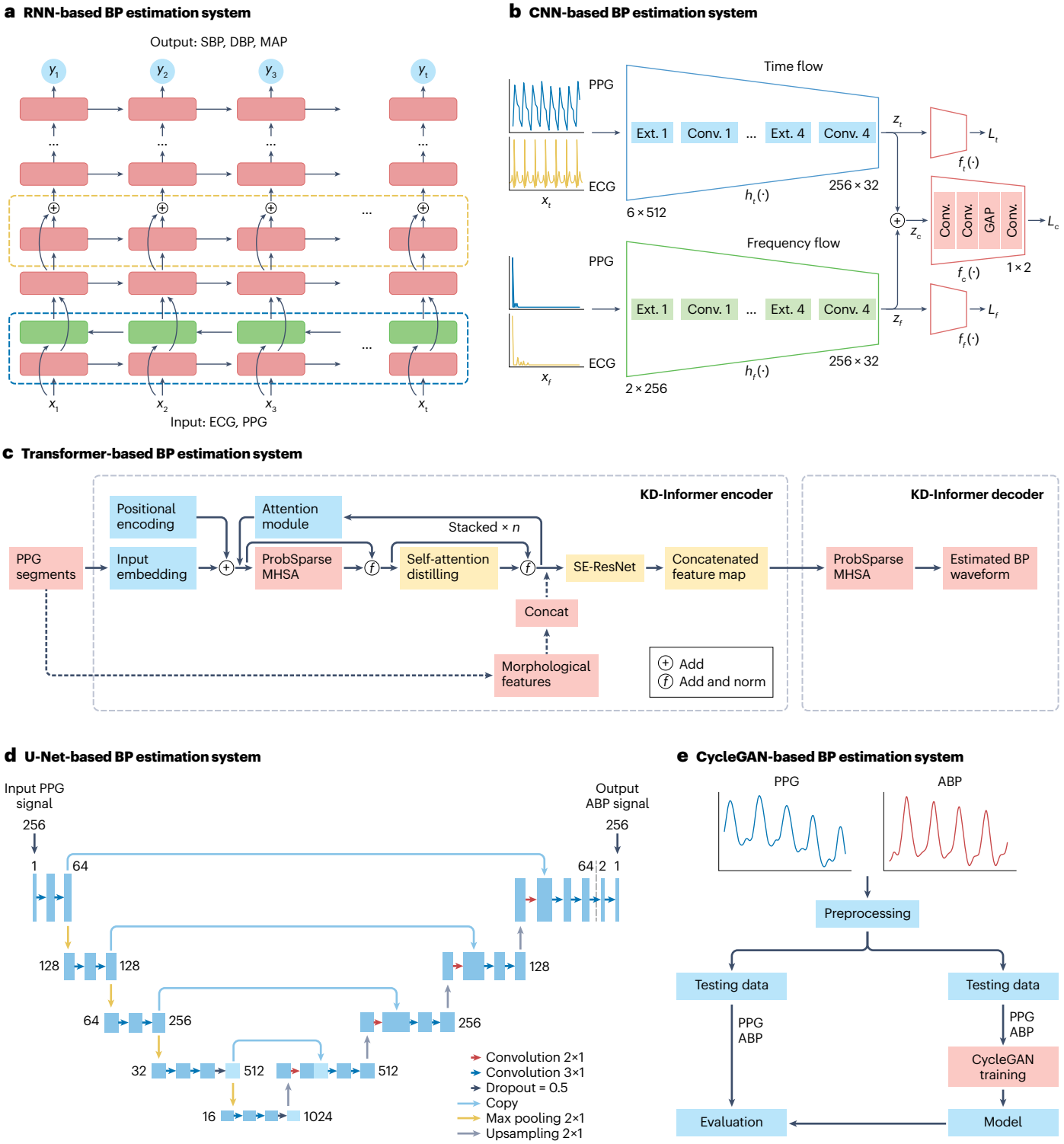

datasets with diverse probability densities. Conversely, HMMs are tailored for sequential data by assuming an underlying Markov process with hidden states, making them especially useful for tasks requiring an understanding of temporal dynamics. For example, a combined GMM–HMM model has been employed to automatically discern and learn the latent structure within auscultatory waveform signals[231].

Advances in deep generative architectures over the past 20 years include autoencoders, U-Net and generative adversarial networks (GANs). Although autoencoders and U-Net are not generative models in the strictest sense, we include them in this category since their adaptations have been effectively used to model the distribution of input data. This usage aligns them with the broader definition of generative

Fig. 4 | Deep learning algorithms for advanced BP estimation. a, Architecture of a recurrent neural network (RNN) comprising long short-term memory (LSTM) layers. The bidirectional LSTM layer (blue dashed border) integrates forward (red boxes) and backward (green boxes) LSTM cells to capture both past and future temporal dependencies in the input temporal signal x, such as electrocardiogram (ECG) and photoplethysmography (PPG). This process is followed by a unidirectional LSTM layer (yellow dashed border), stacked across multiple layers, to predict the corresponding output signal y. **b**, A convolutional neural network (CNN)-based model for blood pressure (BP) estimation. The time flow branch (upper path, X_t) extracts temporal features from the raw signal and the frequency flow branch (lower path, X_f) extracts frequency domain features from the spectral information. Each branch consists of stacked convolution layers: dilated convolution layers for multiscale temporal relation extraction (Ext.) and strided convolution layers (Conv.) for downsampled concentration. Extracted features (z_t, z_f) are fused to predict systolic BP (SBP) and diastolic BP (DBP) through convolutional layers and global average pooling (GAP), with auxiliary predictors (f) optimizing branch-specific temporal and frequency characteristics. The encoders (h_t, h_f) extract features from time and frequency inputs, and the total loss function (L) is designed to enhance model performance by incorporating auxiliary losses. **c**, Architecture of the transformer-based method with knowledge distillation (KD-Informer). The transformer encoder consists of stacked layers comprising input embeddings, attention modules and self-attention distillation. SE-ResNet modules and morphological concatenation are used for refined feature extraction. The KD-Informer decoder reconstructs BP waveforms from the encoded representations. **d**, Architecture of the modified U-Net deep learning model that predicts the non-invasively measured arterial BP signal using the PPG signal. U-Net uses a symmetrical encoder–decoder structure with skip connections, featuring progressive dimensionality reduction followed by upsampling, with intermediate feature maps of specified dimensions, enabling efficient feature extraction and signal reconstruction. **e**, The BP estimation pipeline based on the Cycle Generative Adversarial Network (CycleGAN), which enables unpaired signal-to-signal translation learning. The model learns bidirectional mappings between PPG and arterial blood pressure (ABP) waveforms through dual generator–discriminator pairs, whereby generators produce paired signals from input signals, while the discriminators differentiate between real and generated signals. The framework is optimized with a cycle consistency loss to preserve the underlying structure of the input signals during translation. MAP, mean arterial pressure; MHSA, multihead self-attention. Part **a** adapted with permission from ref. 220, IEEE. Part **b** adapted from ref. 190, CC BY 4.0 (https://creativecommons.org/licenses/by/4.0/). Part **c** adapted with permission from ref. 192, IEEE. Part **d** adapted with permission from ref. 234, CC BY 4.0 (https://creativecommons.org/licenses/by/4.0/). Part **e** adapted with permission from ref. 236, IEEE.

models. Autoencoders employ a neural network with an hourglass-like structure to extract latent features from input data, facilitating the reconstruction of the original input[215]. While these features might be random, generative modelling utilizing autoencoders aims to systematically model the latent distribution of the input. A prominent variant (variational autoencoders) not only captures the structure of the original data distribution but also enables the generation of new, data-like samples from random points within this distribution[232].

U-Net can further improve the autoencoder structure by integrating symmetrical skip connections within its hourglass-like structure, which improves the model's capacity to produce outputs that closely mirror the original data[233]. This design effectively connects deeper and shallower layers, optimizing the flow of information and refining the precision of reconstructions. A U-Net-based architecture has been adapted for translating PPG signals to arterial BP waveform signals, and achieved highly accurate waveform predictions that closely correlate with reference waveforms[234] (Fig. 4d). Furthermore, a shallow 1D U-Net architecture has also been employed for continuous BP monitoring from PPG and ECG signals[235].

GANs are composed of two key modules: a generator and a discriminator. The generator aims to produce real data-like samples from a randomly sampled vector, whereas the discriminator aims to differentiate fake generated data from real data. This setup forms a minimax algorithm, whereby the generator continually improves its ability to produce data indistinguishable from actual data, and the discriminator increases its ability to detect fake data. This competitive dynamic results in the creation of highly realistic data that closely mirrors actual data. However, this dynamic can also lead to unstable training and mode collapse, whereby the generator fails to produce a diverse and realistic data distribution, a key challenge in GANs. A cycle GAN, renowned for its capability in domain translation, has been used to convert clean PPG signals to ambulatory BP[236] (Fig. 4e).

Advances in wearable BP sensors

Research in the field of wearable BP sensors aims to address the limitations of traditional BP monitoring methods, which often rely on bulky, stationary equipment. These technologies focus on facilitating continuous, real-time monitoring to provide more accurate and accessible BP measurements in different environments. Clinical validation studies have demonstrated the potential of these sensors to achieve reliable performance[237,238]. In particular, much research has been dedicated towards improving the materials used in wearable BP sensors, focusing on increasing sensitivity, flexibility and conformal adhesion to the skin. Notable advances include the development of wearable piezoelectric BP sensors (WPBPS) and ultrasonic sensor systems. WPBPS utilize a flexible inorganic piezoelectric PZT film of thickness 2 μm transferred onto a plastic substrate[237] (Fig. 5a). This sensor has shown a linear response with a sensitivity of 0.062 kPa^{-1} for pressures <10 kPa, significantly outperforming conventional flexible piezoelectric sensors[237] (Fig. 5b). The sensor captured pulse waveforms with the maximum and minimum peaks of voltage correlating with SBP and DBP as measured by an oscillometric BP monitor. Based on this correlation, initial calibration was performed by matching the maximum and minimum voltage peaks from the waveforms to the SBP and DBP values from a commercial oscillometric BP monitor through three measurements, and linear regression was used to estimate the BP readings. To verify the accuracy of the WPBPS, a clinical validation study was performed in 35 participants (both healthy individuals and those with hypertension). The mean difference between the WPBPS and a commercial sphygmomanometer was found to be −0.89 ± 6.19 mmHg for SBP and −0.32 ± 5.28 mmHg for DBP, highlighting the accuracy of the WPBPS (Fig. 5c). This WPBPS system, integrated into a wristwatch with a wireless communication circuit, can potentially be used for accurate, convenient and portable BP monitoring[237] (Fig. 5d).

Similarly, advances in wearable ultrasound technology have led to the development of the wearable ultrasound system on a patch (USoP). The USoP integrates a miniaturized, flexible ultrasound probe with control electronics in a wireless format, capturing arterial pulse waveforms and calculating BP using the relationship between arterial diameter changes[142] (Fig. 5e). In the case of wearable ultrasound sensors, BP can be derived by detecting changes in vascular diameter based on the principle outlined in the equation above. However, calibration is

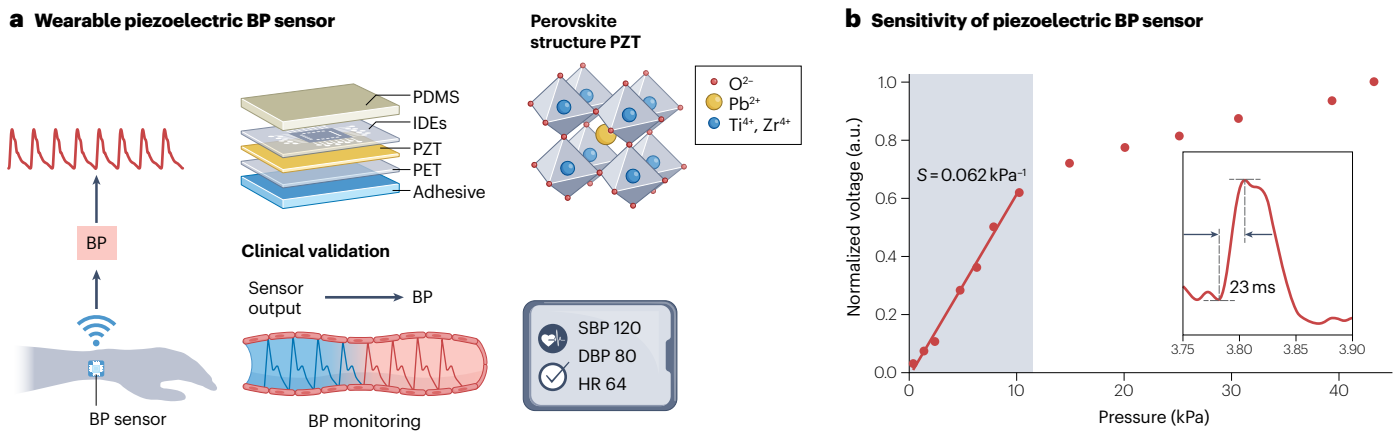
a Wearable piezoelectric BP sensor
BP
BP sensor
PDMS
IDEs
PZT
PET
Adhesive
Clinical validation
Sensor output
BP
BP monitoring
Perovskite structure PZT
O2-
Pb2+
Ti4+, Zr4+
SBP 120
DBP 80
HR 64
b Sensitivity of piezoelectric BP sensor
Normalized voltage (a.u.)
S = 0.062 kPa-1
23 ms
Pressure (kPa)

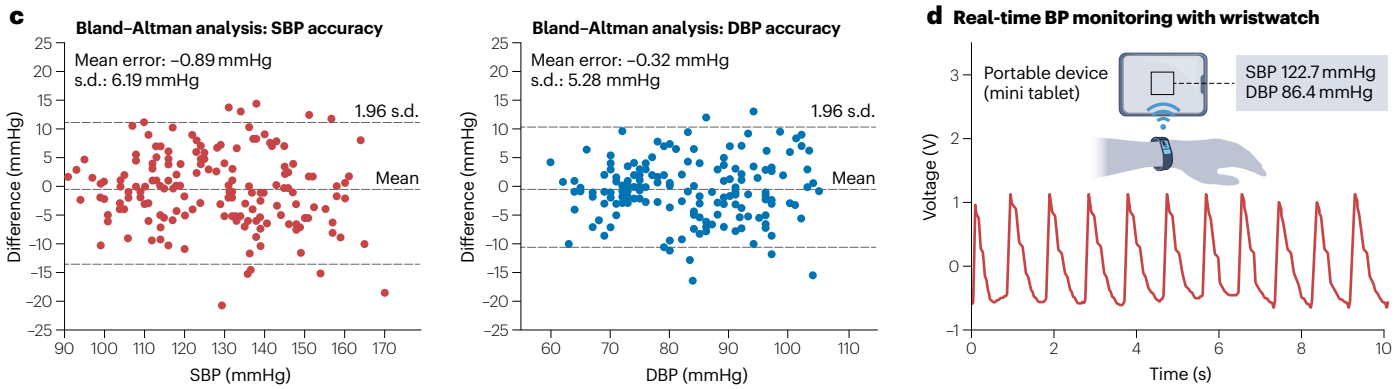
c
Bland–Altman analysis: SBP accuracy
Mean error: −0.89 mmHg
s.d.: 6.19 mmHg
1.96 s.d.
Mean
Difference (mmHg)
SBP (mmHg)
Bland–Altman analysis: DBP accuracy
Mean error: −0.32 mmHg
s.d.: 5.28 mmHg
1.96 s.d.
Mean
DBP (mmHg)
d Real-time BP monitoring with wristwatch
Portable device
(mini tablet)
SBP 122.7 mmHg
DBP 86.4 mmHg
Voltage (V)
Time (s)

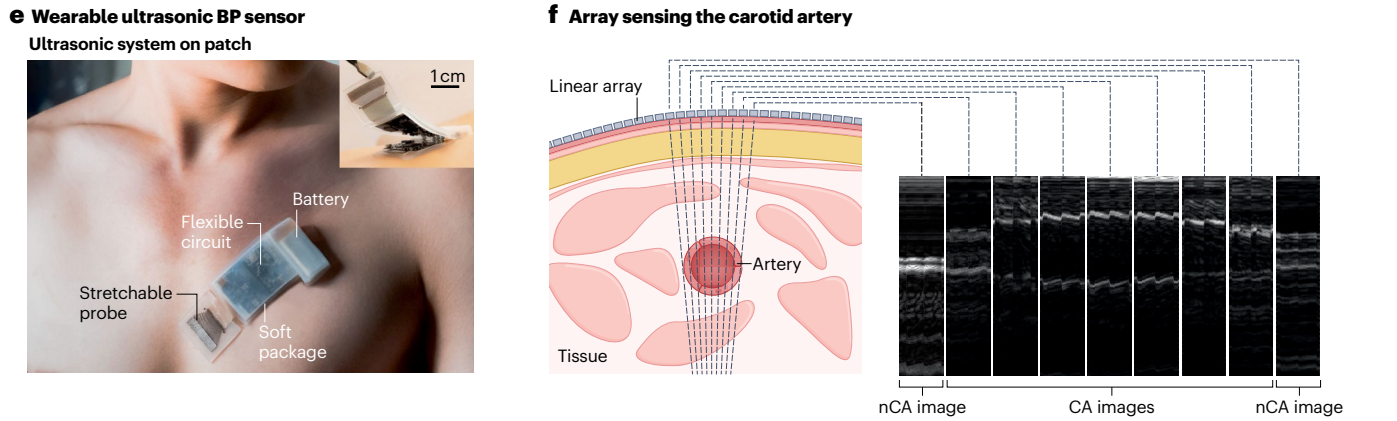
e Wearable ultrasonic BP sensor
Ultrasonic system on patch
1 cm
Battery
Flexible circuit
Stretchable probe
Soft package
f Array sensing the carotid artery
Linear array
Artery
Tissue
nCA image
CA images
nCA image

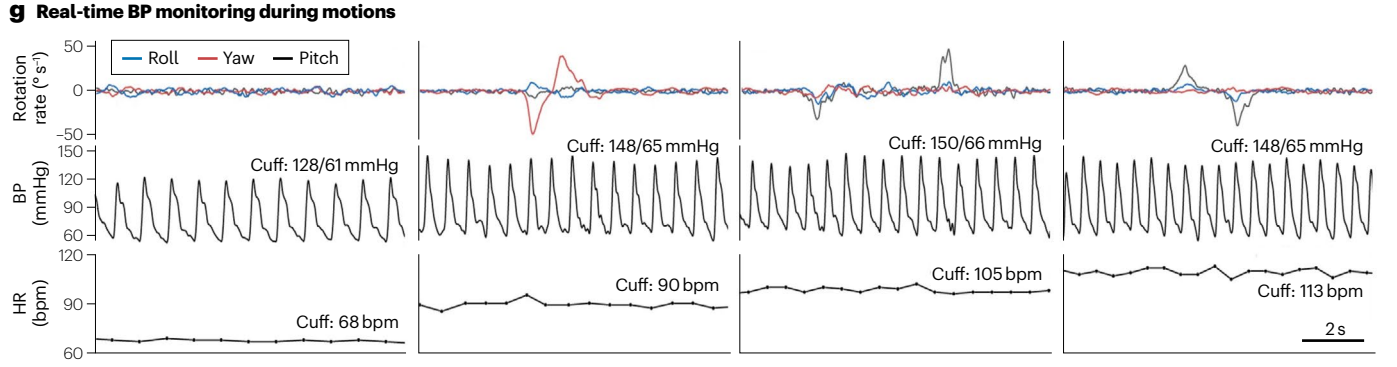
g Real-time BP monitoring during motions
Roll
Yaw
Pitch
Rotation rate (° s-1)
BP (mmHg)
HR (bpm)
Cuff: 128/61 mmHg
Cuff: 148/65 mmHg
Cuff: 150/66 mmHg
Cuff: 148/65 mmHg
Cuff: 68 bpm
Cuff: 90 bpm
Cuff: 105 bpm
Cuff: 113 bpm
2 s

Fig. 5 | Advances in wearable BP sensors. Parts **a**–**d** provide a schematic overview of a wearable piezoelectric blood pressure (BP) sensor. The sensor adheres to the user's skin (part **a**) to accurately detect arterial pulse signals, which are then continuously converted into BP values. The upper insets present the overall layout of the flexible piezoelectric BP sensor and a conceptual image illustrating its clinical validation against a commercial sphygmomanometer. The normalized output voltage (in arbitrary units (a.u.)) as a function of pressure (part **b**), with the sensitivity (*S*) represented as the slope of the output voltage curve, and the rapid response time (23 ms) of the pressure sensor (inset). Bland–Altman plots (part **c**) to validate the accuracy of the wearable piezoelectric BP sensor for systolic BP (SBP) and diastolic BP (DBP) compared with the oscillometric sphygmomanometer in 35 participants. The pulse waveforms (part **d**) are sent from the wristwatch to the portable device via the wireless communication circuit. Parts **e**–**g** provide an overview of a wearable ultrasonic sensor. Photograph of the encapsulated ultrasonic system on patch laminated to the chest (part **e**) for measurement of cardiac activity via the parasternal window. Cross-sectional view of a linear array sensor targeting the carotid artery (CA) (part **f**, left panel). Representative M-mode images illustrating channels where the beam either penetrates or does not penetrate the CA, categorized as CA images or non-CA (nCA) images, respectively. Head movements, BP and heart rate (HR) (part **g**) recorded simultaneously with the ultrasonic system on patch. The carotid DBP measured by the ultrasonic system on patch is in good agreement with the brachial pressures measured by the cuff. IDEs, interdigitated electrodes; PDMS, polydimethylsiloxane; PET, polyethylene terephthalate; PZT, lead zirconate titanate. Parts **a**–**d** adapted with permission from ref. 237, John Wiley and Sons. Parts **e**–**g** adapted from ref. 142, Springer Nature.

required using a commercial BP cuff. Specifically, the constant α in the equation above is calibrated by inputting the actual SBP and DBP values obtained from the cuff, as described in the equation below, allowing the initial calibration and continuous monitoring of BP:

$$\alpha = \frac{A_d \ln\left(\frac{p_s}{p_d}\right)}{A_s - A_d}$$

In this equation, A_s is the systolic arterial cross-section, A_d is the diastolic arterial cross-section, p_s is the systolic pressure and p_d is the diastolic pressure that can be measured using a commercial BP cuff. A 4-MHz 32-channel linear array probe autonomously tracks the position of the carotid artery and senses its pulsations (Fig. 5f). The VGG13 model classifies M-mode images to detect pulsation patterns with precision, recall and accuracy exceeding 98.4%, outperforming other models[142]. This model predicts probability scores for each of the 32 channels, determining the position of the artery by identifying the channel with the highest probability, which is then used to generate pulse waveforms. This system addresses the mobility limitations of traditional ultrasound sensors by enabling real-time monitoring during dynamic activities, such as cycling. ML algorithms are employed to track tissue movements and interpret the data continuously. Validation studies have further demonstrated that the USoP can effectively track physiological signals from tissues as deep as 164 mm and monitor BP, heart rate and cardiac output for up to 12 h in moving individuals[142] (Fig. 5g). This innovation is particularly relevant for clinical settings, given that it can provide reliable data during high-risk activities and offer hands-free, continuous monitoring that extends the capabilities of traditional ultrasound systems[142].

Future directions

The development of cuffless wearable BP sensors has made continuous and non-invasive monitoring possible, but current technology might not yet provide clinically reliable BP measurements, limiting its clinical applicability in routine hypertension management. In acute care settings, such as shock, surgery or intensive care, in which BP fluctuations must be rapidly measured, wearable BP sensors can provide immediate insights for timely intervention. However, further research is needed to improve the reliability of wearable BP sensors, including their ability to accurately infer BP and cardiovascular indicators from waveform signals and ensure effective system integration for reliable data measurement and transmission when attached in wearable form.

Reliability of wearable BP sensors

Several challenges need to be addressed to improve the reliability of cuffless wearable BP sensors, including calibration, motion artefacts and sensor placement, all of which affect BP and cardiovascular indicator accuracy. Overcoming these challenges requires advances in hardware and software, as well as thorough clinical validation.

The reliability of BP sensors can be improved through the use of calibrated pulse waveforms. Continuous monitoring of BP through these calibrated signals offers valuable insights into cardiovascular variables, such as heart rhythm, and enables real-time tracking of BP fluctuations throughout the day. Several studies have explored the relationship between high-precision pulse wave signals from wearable sensors and cardiovascular parameters, such as cardiac output and stroke volume[170,239,240]. Another limitation of current BP sensors is the presence of motion artefacts, which introduce noise into pulsatile signals. Advances in sensor technology and signal processing, such as adaptive filters and ML models, have helped to reduce noise and improve accuracy during movement[241]. In addition, accelerometers assist by filtering out unstable data, ensuring that stable signals are used for BP computation. This combination of motion detection and advanced signal processing is vital for reliable continuous monitoring in dynamic, real-world conditions. Sensor placement also has a crucial role in the reliability of wearable BP sensors. BP sensors are commonly worn on the wrist, and a study has shown that wrist-based BP measurements correlate well with cardiovascular health and can provide valuable insights into arterial health[242]. However, the positioning of sensors in more central locations, such as the carotid artery, might more accurately depict central BP, which is closely linked to cardiovascular outcomes[243]. However, these placements often reduce comfort and wearability, making them less practical for everyday use. Future research should focus on balancing accuracy and comfort by optimizing sensor placement and developing flexible, unobtrusive sensors.

System integration

Effective system integration of wearable BP sensors, which involves integrating sensors, hardware, power supply and wireless communication for accurate real-time data, is essential for their functionality and user acceptance for continuous health monitoring. Furthermore, to increase practicality for daily use and in hospitals, design prototypes should be tailored to specific medical scenarios.

Reliable power sources are crucial for the long-term monitoring capabilities of wearable BP sensors. The latest innovations in power sources for wearable devices include flexible, biocompatible lithium-ion batteries[244,245] and energy harvesting technologies

such as piezoelectric[246,247], triboelectric[74,248] and thermoelectric generators[249,250]. These technologies aim to balance battery size with portability, ensuring continuous use of wearable BP sensors with minimal recharging.

Low-power wireless communication is also crucial for the reliable transmission of data in wearable devices, and includes near-field communication[251,252], Bluetooth technology[253,254] and WiFi[255,256]. Near-field communication is ideal for short-range data transfers with minimal power consumption, whereas Bluetooth Low Energy, which uses identical technology to standard Bluetooth but requires much less energy, provides a balance between power usage and range, making real-time updates possible over moderate distances[175,257,258]. WiFi, particularly newer iterations including WiFi HaLow, offers longer range communication with low power consumption, making it well-suited for medical wearable devices[256]. Advances in radiofrequency power harvesting[259] and wireless power transfer[260,261], such as inductive and resonant inductive coupling, further improve power management for these devices.

Specific design adaptations are required for practical use in daily activities and hospitals[262]. Sensors can be customized for different scenarios, such as 24-h monitoring or for monitoring a hospitalized patient. Each application requires unique features, such as increased durability for continuous use or specialized algorithms for patients with specific physiological conditions. Ensuring efficacy and safety through rigorous clinical trials tailored to specific hospital scenarios is crucial.

Clinical application

The successful clinical integration of wearable BP devices hinges on overcoming key challenges, including ensuring their accuracy and reliability across diverse populations, as well as validating their performance against standard BP measurement techniques. Clinical validation against traditional methods such as auscultatory and oscillometric techniques is crucial. The International Organization for Standardization, the Association for the Advancement of Medical Instrumentation and the British Hypertension Society have established accuracy benchmarks for cuff-based monitors[263], which wearable sensors must not only meet but also exceed, considering their unique characteristics. Diverse participant inclusion in clinical trials is essential to ensure that sensor performance can be tested across different demographics with varying BP conditions. The calibration of these sensors against cuff-based devices and the use of real-time metrics such as 24-h averages and diurnal variations are also key to ensuring accuracy in continuous monitoring.

Conclusions

Wearable BP sensors represent a transformative step in continuous cardiovascular monitoring, leveraging advanced materials and sensing technologies to provide non-invasive, real-time BP estimation. This Review explores the core biosignal acquisition principles underlying these sensors, including mechanoelectric, optoelectronic, ultrasonic and electrophysiological methods. Among these approaches, mechanoelectric sensors, such as piezoelectric and triboelectric devices, offer high sensitivity and flexibility, whereas optoelectronic systems such as PPG provide cost-effective and versatile solutions. Ultrasonic and electrophysiological approaches can enhance precision and extend functionality, particularly for deep-tissue measurements and heart rhythm analysis. BP estimation theories, including PWA, PWV and arterial wall dynamics, highlight the close interplay between cardiovascular mechanics and BP changes, providing robust frameworks for BP monitoring. The integration of ML algorithms further increases accuracy and reliability. ML models, ranging from traditional regression techniques to advanced DL architectures, such as CNN and LSTM networks, have demonstrated their capability to adaptively process complex biosignals, mitigating challenges such as motion artefacts and individual variability.

Advances in wearable BP sensor development from the past decade include innovative material designs, such as flexible piezoelectric sensors and flexible ultrasonic transducers, which improve sensor sensitivity, durability and conformability. System integration has also progressed with the incorporation of wireless communication, ensuring uninterrupted monitoring in diverse settings. Despite these achievements, current wearable BP sensors still face limitations, including calibration challenges, motion artefacts and variability in sensor placement.

To gain widespread acceptance in clinical practice, wearable BP sensors need to be rigorously tested across different populations and conditions. Unlike traditional monitors, these sensors estimate BP through waveform analysis, using pulse waveforms to derive measurements. Factors such as age, skin tone and body composition, and medical conditions such as peripheral vascular disease or arrhythmias, can influence accuracy. However, ML and big data analytics offer solutions by enabling personalized calibration, allowing the sensors to adapt to individual characteristics for more precise readings.

Published online: 18 February 2025

References

1. Lewington, S., Clarke, R., Qizilbash, N., Peto, R. & Collins, R. Age-specific relevance of usual blood pressure to vascular mortality: a meta-analysis of individual data for one million adults in 61 prospective studies. *Lancet* **360**, 1903–1913 (2002).
2. Jones, D. W., Appel, L. J., Sheps, S. G., Roccella, E. J. & Lenfant, C. Measuring blood pressure accurately: new and persistent challenges. *JAMA* **289**, 1027–1030 (2003).
3. Malik, R. et al. Relationship between blood pressure and incident cardiovascular disease: linear and nonlinear Mendelian randomization analyses. *Hypertension* **77**, 2004–2013 (2021).
4. Fuchs, F. D. & Whelton, P. K. High blood pressure and cardiovascular disease. *Hypertension* **75**, 285–292 (2020).
5. Wu, C. Y. et al. High blood pressure and all-cause and cardiovascular disease mortalities in community-dwelling older adults. *Medicine* **94**, e2160 (2015).
6. Perera, Y., Raitt, J., Poole, K., Metcalfe, D. & Lewinsohn, A. Non-invasive versus arterial pressure monitoring in the pre-hospital critical care environment: a paired comparison of concurrently recorded measurements. *Scand. J. Trauma. Resusc. Emerg. Med.* **32**, 77 (2024).
7. Bowdle, T. A. Complications of invasive monitoring. *Anesthesiol. Clin. North. Am.* **20**, 333–350 (2002).
8. Quan, X. et al. Advances in non-invasive blood pressure monitoring. *Sensors* **21**, 4373 (2021).
9. Sladen, A. Complications of invasive hemodynamic monitoring in the intensive care unit. *Curr. Probl. Surg.* **25**, 75–145 (1988).
10. Ramasamy, S. & Balan, A. Wearable sensors for ECG measurement: a review. *Sens. Rev.* **38**, 412–419 (2018).
11. Yoo, J., Yan, L., Lee, S., Kim, H. & Yoo, H. J. A wearable ECG acquisition system with compact planar-fashionable circuit board-based shirt. *IEEE Trans. Inf. Technol. Biomed.* **13**, 897–902 (2009).
12. Lyu, Q., Gong, S., Yin, J., Dyson, J. M. & Cheng, W. Soft wearable healthcare materials and devices. *Adv. Healthc. Mater.* **10**, e2100577 (2021).
13. Shrivastava, S., Trung, T. Q. & Lee, N. E. Recent progress, challenges, and prospects of fully integrated mobile and wearable point-of-care testing systems for self-testing. *Chem. Soc. Rev.* **49**, 1812–1866 (2020).
14. James, G. D. & Gerber, L. M. Measuring arterial blood pressure in humans: auscultatory and automatic measurement techniques for human biological field studies. *Am. J. Hum. Biol.* https://doi.org/10.1002/ajhb.23063 (2018).
15. Kario, K. Sleep and nocturnal hypertension: genes, environment, and individual profiles. *J. Clin. Hypertens.* **24**, 1263–1265 (2022).
16. Tomitani, N., Hoshide, S. & Kario, K. Accurate nighttime blood pressure monitoring with less sleep disturbance. *Hypertens. Res.* **44**, 1671–1673 (2021).
17. Kario, K. Nocturnal hypertension new technology and evidence. *Hypertension* **71**, 997–1009 (2018).

18. Lou, M. et al. Highly wearable, breathable, and washable sensing textile for human motion and pulse monitoring. *ACS Appl. Mater. Interfaces* **12**, 19965–19973 (2020).
19. Kang, X. et al. A wearable and real-time pulse wave monitoring system based on a flexible compound sensor. *Biosensors* **12**, 133 (2022).
20. Huang, Y. et al. Arteriosclerosis assessment based on single-point fingertip pulse monitoring using a wearable iontronic sensor. *Adv. Healthc. Mater.* **12**, e2301838 (2023).
21. Wang, J. et al. Wearable multichannel pulse condition monitoring system based on flexible pressure sensor arrays. *Microsyst. Nanoeng.* **8**, 16 (2022).
22. Su, Y. et al. Muscle fibers inspired high-performance piezoelectric textiles for wearable physiological monitoring. *Adv. Funct. Mater.* **31**, 2010962 (2021).
23. Kim, K. et al. Highly sensitive and wearable liquid metal-based pressure sensor for health monitoring applications: integration of a 3D-printed microbump array with the microchannel. *Adv. Healthc. Mater.* **9**, e2000313 (2019).
24. Castaneda, D., Esparza, A., Ghamari, M., Soltanpur, C. & Nazeran, H. A review on wearable photoplethysmography sensors and their potential future applications in health care. *Int. J. Biosens. Bioelectron.* **4**, 195–202 (2018).
25. Shaltis, P. A., Reisner, A. & Asada, H. H. Wearable, cuff-less PPG-based blood pressure monitor with novel height sensor. *Conf. Proc. IEEE Eng. Med. Biol. Soc.* **2006**, 908–911 (2006).
26. Davies, H. J., Williams, I., Peters, N. S. & Mandic, D. P. In-ear SpO_2: a tool for wearable, unobtrusive monitoring of core blood oxygen saturation. *Sensors* **20**, 4879 (2020).
27. Joo, M. G. et al. Reflection-boosted wearable ring-type pulse oximeters for SpO_2 measurement with high sensitivity and low power consumption. *Biosensors* **13**, 711 (2023).
28. Rodriguez-Labra, J. I., Kosik, C., Maddipatla, D., Narakathu, B. B. & Atashbar, M. Z. Development of a PPG sensor array as a wearable device for monitoring cardiovascular metrics. *IEEE Sens. J.* **21**, 26320–26327 (2021).
29. Steinberg, S., Huang, A., Ono, Y. & Rajan, S. Continuous artery monitoring using a flexible and wearable single-element ultrasonic sensor. *IEEE Instrum. Meas. Mag.* **25**, 6–11 (2022).
30. Huang, A., Yoshida, M., Ono, Y. & Rajan, S. Continuous measurement of arterial diameter using wearable and flexible ultrasonic sensor. *2017 IEEE Int. Ultrason. Symp. (IUS)* 1–4 (IEEE, 2017).
31. Peng, C., Chen, M., Sim, H. K., Zhu, Y. & Jiang, X. Noninvasive and nonocclusive blood pressure monitoring via a flexible piezo-composite ultrasonic sensor. *IEEE Sens. J.* **21**, 2642–2650 (2021).
32. Almohimeed, I., Agarwal, M. & Ono, Y. Wearable ultrasonic sensor using double-layer PVDF films for monitoring tissue motion. *Can. Conf. Electr. Comput. Eng.* https://doi.org/10.1109/CCECE.2018.8447859 (2018).
33. Yin, L. et al. Chest-scale self-compensated epidermal electronics for standard 6-precordial-lead ECG. *NPJ Flex. Electron.* **6**, 29 (2022).
34. Zhang, S. et al. On-skin ultrathin and stretchable multifunctional sensor for smart healthcare wearables. *NPJ Flex. Electron.* **6**, 11 (2022).
35. Han, N. et al. Recent progress of biomaterials-based epidermal electronics for healthcare monitoring and human–machine interaction. *Biosensors* **13**, 393 (2023).
36. Park, C., Chou, P. H., Bai, Y., Matthews, R. & Hibbs, A. An ultra-wearable, wireless, low power ECG monitoring system. *Proceedings of the 2006 IEEE Biomedical Circuits and Systems Conference* pp 241–244 (IEEE, 2006).
37. Zhou, Z. B. et al. Wearable continuous blood pressure monitoring devices based on pulse wave transit time and pulse arrival time: a review. *Materials* **16**, 2133 (2023).
38. Konstantinidis, D. et al. Wearable blood pressure measurement devices and new approaches in hypertension management: the digital era. *J. Hum. Hypertens.* **36**, 945–951 (2022).
39. Islam, S. M. S. et al. Wearable cuffless blood pressure monitoring devices: a systematic review and meta-analysis. *Eur. Hear. J. Digit. Heal.* **3**, 323–337 (2022).
40. Mukkamala, R. et al. Evaluation of the accuracy of cuffless blood pressure measurement devices: challenges and proposals. *Hypertension* **78**, 1161–1167 (2021).
41. Xu, H. et al. A high-sensitivity near-infrared phototransistor based on an organic bulk heterojunction. *Nanoscale* **5**, 11850–11855 (2013).
42. He, J. et al. A universal high accuracy wearable pulse monitoring system via high sensitivity and large linearity graphene pressure sensor. *Nano Energy* **59**, 422–433 (2019).
43. Kang, S. et al. Highly sensitive pressure sensor based on bioinspired porous structure for real-time tactile sensing. *Adv. Electron. Mater*. https://doi.org/10.1002/aelm.201670065 (2016).
44. Li, X. et al. Ultracomfortable hierarchical nanonetwork for highly sensitive pressure sensor. *ACS Nano* **14**, 9605–9612 (2020).
45. Jian, M. et al. Flexible and highly sensitive pressure sensors based on bionic hierarchical structures. *Adv. Funct. Mater*. https://doi.org/10.1002/adfm.201606066 (2017).
46. Barton, C. et al. Evaluation of a machine learning algorithm for up to 48-hour advance prediction of sepsis using six vital signs. *Comput. Biol. Med.* **109**, 79–84 (2019).
47. Gultepe, E. et al. From vital signs to clinical outcomes for patients with sepsis: a machine learning basis for a clinical decision support system. *J. Am. Med. Inform. Assoc.* **21**, 315–325 (2014).
48. Babu, A., Ranpariya, S., Sinha, D. K., Chatterjee, A. & Mandal, D. Deep learning enabled early predicting cardiovascular status using highly sensitive piezoelectric sensor of solution-processable nylon-11. *Adv. Mater. Technol.* **8**, 2202021 (2023).
49. Slapni, Č., Ar, G., Mlakar, N. & Luštrek, M. Blood pressure estimation from photoplethysmogram using a spectro-temporal deep neural network. *Sensors (Switzerland)* **19**, 3420 (2019).
50. Fang, Y. et al. Ambulatory cardiovascular monitoring via a machine-learning-assisted textile triboelectric sensor. *Adv. Mater.* **33**, e2104178 (2021).
51. El-Hajj, C. & Kyriacou, P. A. A review of machine learning techniques in photoplethysmography for the non-invasive cuff-less measurement of blood pressure. *Biomed. Signal. Process. Control.* **58**, 101870 (2020).
52. Homayounfar, S. Z. & Andrew, T. L. Wearable sensors for monitoring human motion: a review on mechanisms, materials, and challenges. *SLAS Technol.* **25**, 9–24 (2020).
53. Park, D. Y. et al. Self-powered real-time arterial pulse monitoring using ultrathin epidermal piezoelectric sensors. *Adv. Mater*. https://doi.org/10.1002/adma.201702308 (2017).
54. Tian, Y., Hu, C., Peng, D. & Zhu, Z. Self-powered intelligent pulse sensor based on triboelectric nanogenerators with AI assistance. *Front. Bioeng. Biotechnol.* **11**, 1236292 (2023).
55. Zhang, F. et al. A highly accurate flexible sensor system for human blood pressure and heart rate monitoring based on graphene/sponge. *RSC Adv.* **12**, 2391–2398 (2022).
56. Mishra, R. B., El-Atab, N., Hussain, A. M. & Hussain, M. M. Recent progress on flexible capacitive pressure sensors: from design and materials to applications. *Adv. Mater. Technol.* **6**, 2001023 (2021).
57. Sun, Q. et al. Active matrix electronic skin strain sensor based on piezopotential-powered graphene transistors. *Adv. Mater.* **27**, 3411–3417 (2015).
58. Dagdeviren, C. et al. Conformable amplified lead zirconate titanate sensors with enhanced piezoelectric response for cutaneous pressure monitoring. *Nat. Commun.* **5**, 4496 (2014).
59. Chu, Y. et al. Human pulse diagnosis for medical assessments using a wearable piezoelectret sensing system. *Adv. Funct. Mater.* **28**, 1803413 (2018).
60. Tamura, T., Maeda, Y., Sekine, M. & Yoshida, M. Wearable photoplethysmographic sensors – past and present. *Electron* **3**, 282–302 (2014).
61. Hu, H. et al. Stretchable ultrasonic transducer arrays for three-dimensional imaging on complex surfaces. *Sci. Adv.* **4**, eaar3979 (2018).
62. Meziane, N., Webster, J. G., Attari, M. & Nimunkar, A. J. Dry electrodes for electrocardiography. *Physiol. Meas.* **34**, R47–R69 (2013).
63. Donelan, J. M. et al. Biomechanical energy harvesting: generating electricity during walking with minimal user effort. *Science* **319**, 807–810 (2008).
64. Damjanovic, D. Ferroelectric, dielectric and piezoelectric properties of ferroelectric thin films and ceramics. *Rep. Prog. Phys.* **61**, 1267–1324 (1998).
65. Fu, H. & Cohen, R. E. Polarization rotation mechanism for ultrahigh electromechanical response. *Nature* **403**, 281–283 (2000).
66. Tressler, J. F., Alkoy, S. & Newnham, R. E. Piezoelectric sensors and sensor materials. *J. Electroceram.* **2**, 257–272 (1998).
67. Wan, C. & Bowen, C. R. Multiscale-structuring of polyvinylidene fluoride for energy harvesting: the impact of molecular-, micro- and macro-structure. *J. Mater. Chem. A* **5**, 3091–3128 (2017).
68. Park, K. II et al. Highly-efficient, flexible piezoelectric PZT thin film nanogenerator on plastic substrates. *Adv. Mater.* **26**, 2514–2520 (2014).
69. Kabra, H., Deore, H. A. & Patil, P. Review on advanced piezoelectric materials ($BaTiO_3$, PZT). *JETIR* **6**, 950–957 (2019).
70. Kim, M., Doh, I., Oh, E. & Cho, Y. H. Flexible piezoelectric pressure sensors fabricated from nanocomposites with enhanced dispersion and vapor permeability for precision pulse wave monitoring. *ACS Appl. Nano Mater.* **6**, 22025–22035 (2023).
71. Chun, K. Y., Seo, S. & Han, C. S. A wearable all-gel multimodal cutaneous sensor enabling simultaneous single-site monitoring of cardiac-related biophysical signals. *Adv. Mater.* **34**, e2110082 (2022).
72. Yang, T. et al. Hierarchically structured PVDF/ZnO core-shell nanofibers for self-powered physiological monitoring electronics. *Nano Energy* **72**, 104706 (2020).
73. Tian, G. et al. Hierarchical piezoelectric composites for noninvasive continuous cardiovascular monitoring. *Adv. Mater.* **36**, 2313612 (2024).
74. Xiao, X., Chen, G., Libanori, A. & Chen, J. Wearable triboelectric nanogenerators for therapeutics. *Trends Chem.* **3**, 279–290 (2021).
75. Wang, Z. L., Chen, J. & Lin, L. Progress in triboelectric nanogenerators as a new energy technology and self-powered sensors. *Energy Environ. Sci.* **8**, 2250–2282 (2015).
76. Wang, H. S. et al. Performance-enhanced triboelectric nanogenerator enabled by wafer-scale nanogrates of multistep pattern downscaling. *Nano Energy* **35**, 415–423 (2017).
77. Lee, B. Y., Kim, S. U., Kang, S. & Lee, S. D. Transparent and flexible high power triboelectric nanogenerator with metallic nanowire-embedded tribonegative conducting polymer. *Nano Energy* **53**, 152–159 (2018).
78. Jeong, C. K. et al. Topographically-designed triboelectric nanogenerator via block copolymer self-assembly. *Nano Lett.* **14**, 7031–7038 (2014).
79. Kim, D. et al. Direct-laser-patterned friction layer for the output enhancement of a triboelectric nanogenerator. *Nano Energy* **35**, 379–386 (2017).
80. Meng, K. et al. Kirigami-inspired pressure sensors for wearable dynamic cardiovascular monitoring. *Adv. Mater.* **34**, e2202478 (2022).
81. Park, H. W. et al. Electron blocking layer-based interfacial design for highly-enhanced triboelectric nanogenerators. *Nano Energy* **50**, 9–15 (2018).
82. Chai, B. et al. Conductive interlayer modulated ferroelectric nanocomposites for high performance triboelectric nanogenerator. *Nano Energy* **91**, 106668 (2022).
83. Kim, D. W., Lee, J. H., You, I., Kim, J. K. & Jeong, U. Adding a stretchable deep-trap interlayer for high-performance stretchable triboelectric nanogenerators. *Nano Energy* **50**, 192–200 (2018).
84. Yu, Y. & Wang, X. Chemical modification of polymer surfaces for advanced triboelectric nanogenerator development. *Extrem. Mech. Lett.* **9**, 514–530 (2016).

85. Chen, G., Au, C. & Chen, J. Textile triboelectric nanogenerators for wearable pulse wave monitoring. *Trends Biotechnol.* **39**, 1078–1092 (2021).
86. Dong, K. et al. A stretchable yarn embedded triboelectric nanogenerator as electronic skin for biomechanical energy harvesting and multifunctional pressure sensing. *Adv. Mater.* **30**, e1804944 (2018).
87. Lin, Z. et al. Triboelectric nanogenerator enabled body sensor network for self-powered human heart-rate monitoring. *ACS Nano* **11**, 8830–8837 (2017).
88. Ouyang, H. et al. Self-powered pulse sensor for antidiastole of cardiovascular disease. *Adv. Mater.* **29**, 1703456 (2017).
89. Fan, W. et al. Machine-knitted washable sensor array textile for precise epidermal physiological signal monitoring. *Sci. Adv.* **6**, eaay2840 (2020).
90. Yue, Y. et al. 3D hybrid porous Mxene-sponge network and its application in piezoresistive sensor. *Nano Energy* **50**, 79–87 (2018).
91. Fiorillo, A. S., Critello, C. D. & Pullano, A. S. Theory, technology and applications of piezoresistive sensors: a review. *Sens. Actuat. A Phys.* **281**, 156–175 (2018).
92. Choong, C. L. et al. Highly stretchable resistive pressure sensors using a conductive elastomeric composite on a micropyramid array. *Adv. Mater.* **26**, 3451–3458 (2014).
93. Fang, X. et al. High-performance MXene-based flexible and wearable pressure sensor based on a micro-pyramid structured active layer. *Adv. Mater. Technol.* **8**, 2200291 (2023).
94. Pang, C. et al. A flexible and highly sensitive strain-gauge sensor using reversible interlocking of nanofibres. *Nat. Mater.* **11**, 795–801 (2012).
95. Pan, L. et al. An ultra-sensitive resistive pressure sensor based on hollow-sphere microstructure induced elasticity in conducting polymer film. *Nat. Commun.* **5**, 3002 (2014).
96. Bijender, N. et al. Noninvasive blood pressure monitoring via a flexible and wearable piezoresistive sensor. *ACS Omega* **9**, 6355–6365 (2024).
97. Yao, H. et al. A flexible and highly pressure-sensitive graphene–polyurethane sponge based on fractured microstructure design. *Adv. Mater.* **25**, 6692–6698 (2013).
98. Liu, C. et al. High-performance piezoresistive flexible pressure sensor based on wrinkled microstructures prepared from discarded vinyl records and ultra-thin, transparent polyaniline films for human health monitoring. *J. Mater. Chem. C.* **10**, 13064–13073 (2022).
99. Luo, R. et al. Fragmented graphene aerogel/polydimethylsiloxane sponges for wearable piezoresistive pressure sensors. *ACS Appl. Nano Mater.* **6**, 7065–7076 (2023).
100. Xu, H. et al. Flexible waterproof piezoresistive pressure sensors with wide linear working range based on conductive fabrics. *Nanomicro Lett.* **12**, 159 (2020).
101. Zheng, Y. et al. Conductive MXene/cotton fabric based pressure sensor with both high sensitivity and wide sensing range for human motion detection and E-skin. *Chem. Eng. J.* **420**, 127720 (2021).
102. Ding, X. et al. Highly accurate wearable piezoresistive sensors without tension disturbance based on weaved conductive yarn. *ACS Appl. Mater. Interfaces* **12**, 35638–35646 (2020).
103. Yang, X., Wang, Y. & Qing, X. A flexible capacitive pressure sensor based on ionic liquid. *Sensors* **18**, 2395 (2018).
104. Zhang, Z. et al. Highly sensitive capacitive pressure sensor based on a micropyramid array for health and motion monitoring. *Adv. Electron. Mater.* **7**, 2100174 (2021).
105. Yang, J. C. et al. Microstructured porous pyramid-based ultrahigh sensitive pressure sensor insensitive to strain and temperature. *ACS Appl. Mater. Interfaces* **11**, 19472–19480 (2019).
106. Ruth, S. R. A. et al. Rational design of capacitive pressure sensors based on pyramidal microstructures for specialized monitoring of biosignals. *Adv. Funct. Mater.* **30**, 1903100 (2020).
107. Ruth, S. R. A., Feig, V. R., Tran, H. & Bao, Z. Microengineering pressure sensor active layers for improved performance. *Adv. Funct. Mater.* **30**, 2003491 (2020).
108. Kim, J. O. et al. Highly ordered 3D microstructure-based electronic skin capable of differentiating pressure, temperature, and proximity. *ACS Appl. Mater. Interfaces* **11**, 1503–1511 (2019).
109. Wei, P., Guo, X., Qiu, X. & Yu, D. Flexible capacitive pressure sensor with sensitivity and linear measuring range enhanced based on porous composite of carbon conductive paste and polydimethylsiloxane. *Nanotechnology* **30**, 455501 (2019).
110. Wang, S. et al. High sensitivity capacitive flexible pressure sensor based on PDMS double wrinkled microstructure. *J. Mater. Sci. Mater. Electron.* **35**, 78 (2024).
111. Joo, Y. et al. Silver nanowire-embedded PDMS with a multiscale structure for a highly sensitive and robust flexible pressure sensor. *Nanoscale* **7**, 6208–6215 (2015).
112. Bisri, S. Z., Shimizu, S., Nakano, M. & Iwasa, Y. Endeavor of iontronics: from fundamentals to applications of ion-controlled electronics. *Adv. Mater.* https://doi.org/10.1002/adma.201607054 (2017).
113. Liu, Q. et al. Highly transparent and flexible iontronic pressure sensors based on an opaque to transparent transition. *Adv. Sci.* https://doi.org/10.1002/advs.202000348 (2020).
114. Bai, N. et al. Graded intrafillable architecture-based iontronic pressure sensor with ultra-broad-range high sensitivity. *Nat. Commun.* **11**, 209 (2020).
115. Lee, G. H. et al. Multifunctional materials for implantable and wearable photonic healthcare devices. *Nat. Rev. Mater.* **5**, 149–165 (2020).
116. Kim, K. B. & Baek, H. J. Photoplethysmography in wearable devices: a comprehensive review of technological advances, current challenges, and future directions. *Electronics* **12**, 2923 (2023).
117. Tamura, T. Current progress of photoplethysmography and SPO_2 for health monitoring. *Biomed. Eng. Lett.* **9**, 21–36 (2019).
118. Lee, I. et al. Systematic review on human skin-compatible wearable photoplethysmography sensors. *Appl. Sci.* **11**, 2313 (2021).
119. Lee, H. et al. Toward all-day wearable health monitoring: an ultralow-power, reflective organic pulse oximetry sensing patch. *Sci. Adv.* **4**, eaas9530 (2018).
120. Khan, Y. et al. A flexible organic reflectance oximeter array. *Proc. Natl Acad. Sci. USA* **115**, E11015–E11024 (2018).
121. Lochner, C. M., Khan, Y., Pierre, A. & Arias, A. C. All-organic optoelectronic sensor for pulse oximetry. *Nat. Commun.* **5**, 5745 (2014).
122. Yokota, T. et al. Ultraflexible organic photonic skin. *Sci. Adv.* **2**, e1501856 (2016).
123. Han, D. et al. Flexible blade-coated multicolor polymer light-emitting diodes for optoelectronic sensors. *Adv. Mater.* **29**, 1606206 (2017).
124. Jinno, H. et al. Self-powered ultraflexible photonic skin for continuous bio-signal detection via air-operation-stable polymer light-emitting diodes. *Nat. Commun.* **12**, 2234 (2021).
125. Xu, H. et al. Flexible organic/inorganic hybrid near-infrared photoplethysmogram sensor for cardiovascular monitoring. *Adv. Mater.* https://doi.org/10.1002/adma.201700975 (2017).
126. Bent, B., Goldstein, B. A., Kibbe, W. A. & Dunn, J. P. Investigating sources of inaccuracy in wearable optical heart rate sensors. *NPJ Digit. Med.* **3**, 18 (2020).
127. Maeda, Y., Sekine, M. & Tamura, T. Relationship between measurement site and motion artifacts in wearable reflected photoplethysmography. *J. Med. Syst.* **35**, 969–976 (2011).
128. D'Orazio, J., Jarrett, S., Amaro-Ortiz, A. & Scott, T. UV radiation and the skin. *Int. J. Mol. Sci.* **14**, 12222–12248 (2013).
129. Boonya-ananta, T. et al. Synthetic photoplethysmography (PPG) of the radial artery through parallelized Monte Carlo and its correlation to body mass index (BMI). *Sci. Rep.* **11**, 2570 (2021).
130. Kim, J., Lee, T., Kim, J. & Ko, H. Ambient light cancellation in photoplethysmogram application using alternating sampling and charge redistribution technique. *Annu. Int. Conf. IEEE Eng. Med. Biol. Soc.* **2015**, 6441–6444 (2015).
131. Allen, J., Frame, J. R. & Murray, A. Microvascular blood flow and skin temperature changes in the fingers following a deep inspiratory gasp. *Physiol. Meas.* **23**, 365–373 (2002).
132. Chong, J. W. et al. Photoplethysmograph signal reconstruction based on a novel hybrid motion artifact detection–reduction approach. Part I: motion and noise artifact detection. *Ann. Biomed. Eng.* **42**, 2238–2250 (2014).
133. Charlton, P. H. et al. An assessment of algorithms to estimate respiratory rate from the electrocardiogram and photoplethysmogram. *Physiol. Meas.* **37**, 610–626 (2016).
134. Franklin, D. et al. Synchronized wearables for the detection of haemodynamic states via electrocardiography and multispectral photoplethysmography. *Nat. Biomed. Eng.* **7**, 1229–1241 (2023).
135. Khan, E., Al Hossain, F., Uddin, S. Z., Alam, S. K. & Hasan, M. K. A robust heart rate monitoring scheme using photoplethysmographic signals corrupted by intense motion artifacts. *IEEE Trans. Biomed. Eng.* **63**, 550–562 (2016).
136. Lee, H., Chung, H., Kim, J. W. & Lee, J. Motion artifact identification and removal from wearable reflectance photoplethysmography using piezoelectric transducer. *IEEE Sens. J.* **19**, 3861–3870 (2019).
137. Wang, C. et al. Continuous monitoring of deep-tissue haemodynamics with stretchable ultrasonic phased arrays. *Nat. Biomed. Eng.* **5**, 749–758 (2021).
138. Pang, D. C. & Chang, C. M. Development of a novel transparent flexible capacitive micromachined ultrasonic transducer. *Sensors* **17**, 1443 (2017).
139. Kruizinga, P. et al. Compressive 3D ultrasound imaging using a single sensor. *Sci. Adv.* **3**, e170143 (2017).
140. Lin, M., Hu, H., Zhou, S. & Xu, S. Soft wearable devices for deep-tissue sensing. *Nat. Rev. Mater.* **7**, 850–869 (2022).
141. Wang, C. C. et al. Monitoring of the central blood pressure waveform via a conformal ultrasonic device. *Nat. Biomed. Eng.* **2**, 687–695 (2018).
142. Lin, M. et al. A fully integrated wearable ultrasound system to monitor deep tissues in moving subjects. *Nat. Biotechnol.* **42**, 448–457 (2024).
143. Hu, H. et al. A wearable cardiac ultrasound imager. *Nature* **613**, 667–675 (2023).
144. Sempionatto, J. R. et al. An epidermal patch for the simultaneous monitoring of haemodynamic and metabolic biomarkers. *Nat. Biomed. Eng.* **5**, 737–748 (2021).
145. Hu, H. et al. Stretchable ultrasonic arrays for the three-dimensional mapping of the modulus of deep tissue. *Nat. Biomed. Eng.* **7**, 1321–1334 (2023).
146. Gao, X. et al. A photoacoustic patch for three-dimensional imaging of hemoglobin and core temperature. *Nat. Commun.* **13**, 7757 (2022).
147. Padala, S. K., Cabrera, J. A. & Ellenbogen, K. A. Anatomy of the cardiac conduction system. *Pacing Clin. Electrophysiol.* **44**, 15–25 (2021).
148. Becker, D. E. Fundamentals of electrocardiography interpretation. *Anesth. Prog.* **53**, 53–64 (2006).
149. Veeraraghavan, R., Gourdie, R. G. & Poelzing, S. Mechanisms of cardiac conduction: a history of revisions. *Am. J. Physiol. Heart Circ. Physiol.* **306**, H619–H627 (2014).
150. Martis, R. J., Acharya, U. R. & Adeli, H. Current methods in electrocardiogram characterization. *Comput. Biol. Med.* **48**, 133–149 (2014).
151. Homsy, J. & Podrid, P. J. in *MGH Cardiology Board Review* (eds Gaggin, H. & Januzzi, J., Jr.) 580–622 (Springer, 2014).
152. AlGhatrif, M. & Lindsay, J. A brief review: history to understand fundamentals of electrocardiography. *J. Community Hosp. Intern. Med. Perspect.* **2**, 14383 (2012).
153. Lujan, M. R., Perez-Pozuelo, I. & Grandner, M. A. Past, present, and future of multisensory wearable technology to monitor sleep and circadian rhythms. *Front. Digit. Heal.* **3**, 721919 (2021).
154. Searle, A. & Kirkup, L. A direct comparison of wet, dry and insulating bioelectric recording electrodes. *Physiol. Meas.* **21**, 271–283 (2000).
155. Lim, C. et al. Tissue-like skin-device interface for wearable bioelectronics by using ultrasoft, mass-permeable, and low-impedance hydrogels. *Sci. Adv.* **7**, eabd6716 (2021).

156. Ha, M., Lim, S. & Ko, H. Wearable and flexible sensors for user-interactive health-monitoring devices. *J. Mater. Chem. B* **6**, 4043–4064 (2018).
157. Gao, W., Ota, H., Kiriya, D., Takei, K. & Javey, A. Flexible electronics toward wearable sensing. *Acc. Chem. Res.* **52**, 523–533 (2019).
158. Ling, Y. et al. Disruptive, soft, wearable sensors. *Adv. Mater.* **32**, e1904664 (2020).
159. Ma, Z. et al. Permeable superelastic liquid-metal fibre mat enables biocompatible and monolithic stretchable electronics. *Nat. Mater.* **20**, 859–868 (2021).
160. Son, D. et al. An integrated self-healable electronic skin system fabricated via dynamic reconstruction of a nanostructured conducting network. *Nat. Nanotechnol.* **13**, 1057–1065 (2018).
161. Zhang, L. et al. Fully organic compliant dry electrodes self-adhesive to skin for long-term motion-robust epidermal biopotential monitoring. *Nat. Commun.* **11**, 4683 (2020).
162. Chen, X. et al. Fabric-substrated capacitive biopotential sensors enhanced by dielectric nanoparticles. *Nano Res.* **14**, 3248–3252 (2021).
163. Jeong, J. W. et al. Capacitive epidermal electronics for electrically safe, long-term electrophysiological measurements. *Adv. Healthc. Mater.* **3**, 642–648 (2014).
164. Liu, J., Hahn, J. O. & Mukkamala, R. Error mechanisms of the oscillometric fixed-ratio blood pressure measurement method. *Ann. Biomed. Eng.* **41**, 587–597 (2013).
165. Colquhoun, D., Dunn, L. K., McMurry, T. & Thiele, R. H. The relationship between the area of peripherally-derived pressure volume loops and systemic vascular resistance. *J. Clin. Monit. Comput.* **27**, 689–696 (2013).
166. Kwon, H. M. et al. Estimation of stroke volume variance from arterial blood pressure: using a 1-D convolutional neural network. *Sensors* **21**, 5130 (2021).
167. Solà, J. & Delgado-Gonzalo, R. *The Handbook of Cuffless Blood Pressure Monitoring: A Guide for Clinicians, Researchers, and Engineers* (Springer, 2019).
168. Wołos, K. et al. Non-invasive assessment of stroke volume and cardiovascular parameters based on peripheral pressure waveform. *PLoS Comput. Biol.* **20**, e1012013 (2024).
169. Kim, J. et al. Soft wearable pressure sensors for beat-to-beat blood pressure monitoring. *Adv. Healthc. Mater.* **8**, e1900109 (2019).
170. Li, S. et al. Monitoring blood pressure and cardiac function without positioning via a deep learning–assisted strain sensor array. *Sci. Adv.* **9**, eadh0615 (2023).
171. Yi, Z. et al. Piezoelectric dynamics of arterial pulse for wearable continuous blood pressure monitoring. *Adv. Mater.* **34**, e2110291 (2022).
172. Yao, Y. et al. Estimation of central pulse wave velocity from radial pulse wave analysis. *Comput. Methods Prog. Biomed.* **219**, 106781 (2022).
173. Mishra, B. & Thakkar, N. Cuffless blood pressure monitoring using PTT and PWV methods. *Proceedings of the 2017 International Conference on Recent Innovations in Signal Processing and Embedded Systems* pp 395–401 (IEEE, 2017).
174. Ma, Y. et al. Relation between blood pressure and pulse wave velocity for human arteries. *Proc. Natl Acad. Sci. USA* **115**, 11144–11149 (2018).
175. Chung, H. U. et al. Skin-interfaced biosensors for advanced wireless physiological monitoring in neonatal and pediatric intensive-care units. *Nat. Med.* **26**, 418–429 (2020).
176. Liu, C. et al. Wireless, skin-interfaced devices for pediatric critical care: application to continuous, noninvasive blood pressure monitoring. *Adv. Healthc. Mater.* **10**, e2100383 (2021).
177. Yoon, Y. Z. et al. Cuff-less blood pressure estimation using pulse waveform analysis and pulse arrival time. *IEEE J. Biomed. Heal. Inform.* **22**, 1068–1074 (2018).
178. Zhang, G., Gao, M., Xu, D., Olvier, N. B. & Mukkamala, R. Pulse arrival time is not an adequate surrogate for pulse transit time as a marker of blood pressure. *J. Appl. Physiol.* **111**, 1681–1686 (2011).
179. Carek, A. M., Conant, J., Joshi, A., Kang, H. & Inan, O. T. SeismoWatch: wearable cuffless blood pressure monitoring using pulse transit time. *Proc. ACM Interact. Mob. Wearable Ubiquitous Technol.* **1**, 40 (2017).
180. Li, H. et al. Wearable skin-like optoelectronic systems with suppression of motion artifacts for cuff-less continuous blood pressure monitor. *Natl. Sci. Rev.* **7**, 849–862 (2020).
181. Meng, K. et al. Flexible weaving constructed self-powered pressure sensor enabling continuous diagnosis of cardiovascular disease and measurement of cuffless blood pressure. *Adv. Funct. Mater.* **29**, 1806388 (2019).
182. Proença, J., Muehlsteff, J., Aubert, X. & Carvalho, P. Is pulse transit time a good indicator of blood pressure changes during short physical exercise in a young population? *Annu. Int. Conf. IEEE Eng. Med. Biol. Soc.* **2010**, 598–601 (2010).
183. Elgendi, M. et al. The use of photoplethysmography for assessing hypertension. *NPJ Digit. Med.* **2**, 60 (2019).
184. Baier, D., Teren, A., Wirkner, K., Loeffler, M. & Scholz, M. Parameters of pulse wave velocity: determinants and reference values assessed in the population-based study LIFE-Adult. *Clin. Res. Cardiol.* **107**, 1050–1061 (2018).
185. Pereira, T., Correia, C. & Cardoso, J. Novel methods for pulse wave velocity measurement. *J. Med. Biol. Eng.* **35**, 555–565 (2015).
186. Gao, S. C., Wittek, P., Zhao, L. & Jiang, W. J. Data-driven estimation of blood pressure using photoplethysmographic signals. *Proceedings of the 2016 38th Annual International Conference of the IEEE Engineering in Medicine and Biology Society* pp 766–769 (IEEE, 2016).
187. He, R. et al. Beat-to-beat ambulatory blood pressure estimation based on random forest. *Proceedings of the 2016 IEEE 13th International Conference on Wearable and Implantable Body Sensor Networks (BSN)* pp 194–198 (IEEE, 2016).
188. Suzuki, S. & Oguri, K. Cuffless blood pressure estimation by error-correcting output coding method based on an aggregation of AdaBoost with a photoplethysmograph sensor. *Proceedings of the 2009 Annual International Conference of the IEEE Engineering in Medicine and Biology Society* pp 6765–6768 (IEEE, 2009).
189. Sideris, C., Kalantarian, H., Nemati, E. & Sarrafzadeh, M. Building continuous arterial blood pressure prediction models using recurrent networks. *Proceedings of the 2016 IEEE International Conference on Smart Computing (SMARTCOMP)* pp 1–5 (IEEE, 2016).
190. Baek, S., Jang, J. & Yoon, S. End-to-end blood pressure prediction via fully convolutional networks. *IEEE Access.* **7**, 185458–185468 (2019).
191. Jeong, D. U. & Lim, K. M. Combined deep CNN–LSTM network-based multitasking learning architecture for noninvasive continuous blood pressure estimation using difference in ECG-PPG features. *Sci. Rep.* **11**, 13539 (2021).
192. Ma, C. et al. KD-informer: a cuff-less continuous blood pressure waveform estimation approach based on single photoplethysmography. *IEEE J. Biomed. Heal. Inform.* **27**, 2219–2230 (2023).
193. Mieloszyk, R. et al. A comparison of wearable tonometry, photoplethysmography, and electrocardiography for cuffless measurement of blood pressure in an ambulatory setting. *IEEE J. Biomed. Heal. Inform.* **26**, 2864–2875 (2022).
194. Duan, K., Qian, Z., Atef, M. & Wang, G. A feature exploration methodology for learning based cuffless blood pressure measurement using photoplethysmography. *Proceedings of the 2016 38th Annual International Conference of the IEEE Engineering in Medicine and Biology Society* pp 6385–6388 (IEEE, 2016).
195. Kachuee, M., Kiani, M. M., Mohammadzade, H. & Shabany, M. Cuffless blood pressure estimation algorithms for continuous health-care monitoring. *IEEE Trans. Biomed. Eng.* **64**, 859–869 (2017).
196. Goli, S. & Jayanthi, T. Cuff less continuous non-invasive blood pressure measurement using pulse transit time measurement. *Int. J. Recent. Dev. Eng. Technol.* **2**, 86–91 (2014).
197. Mousavi, S. S. et al. Cuff-less blood pressure estimation using only the ECG signal in frequency domain. *Proceedings of the 2018 8th International Conference on Computer and Knowledge Engineering (ICCKE)* pp 147–152 (IEEE, 2018).
198. Cattivelli, F. S. & Garudadri, H. Noninvasive cuffless estimation of blood pressure from pulse arrival time and heart rate with adaptive calibration. *Proceedings of the 2009 Sixth International Workshop on Wearable and Implantable Body Sensor Networks* pp 114–119 (IEEE, 2009).
199. Zhang, B., Ren, H., Huang, G., Cheng, Y. & Hu, C. Predicting blood pressure from physiological index data using the SVR algorithm 08 information and computing sciences 0801 artificial intelligence and image processing. *BMC Bioinforma.* **20**, 109 (2019).
200. Yi, C., Jian, C. & Wenqiang, J. Continuous blood pressure measurement based on photoplethysmography. *Proceedings of the 2019 14th IEEE International Conference on Electronic Measurement and Instruments (ICEMI)* pp 1656–1663 (2019).
201. Khalid, S. G., Zhang, J., Chen, F. & Zheng, D. Blood pressure estimation using photoplethysmography only: comparison between different machine learning approaches. *J. Healthc. Eng.* **2018**, 1548647 (2018).
202. Krizhevsky, A., Sutskever, I. & Hinton, G. E. ImageNet classification with deep convolutional neural networks. *Commun. ACM* **60**, 84–90 (2017).
203. Hattiya, T., Dittakan, K. & Musikasuwan, S. Diabetic retinopathy detection using convolutional neural network: a comparative study on different architectures. *Eng. Access.* **7**, 50–60 (2021).
204. Liu, Z. et al. A ConvNet for the 2020s. *Proceedings of the 2022 IEEE/CVF Conference on Computer Vision and Pattern Pattern Recogniti*on pp 11966–11976 (IEEE, 2022).
205. Woo, S. et al. ConvNeXt V2: co-designing and scaling ConvNets with masked autoencoders. *Proceedings of the 2023 IEEE/CVF Conference on Computer Vision and Pattern Recognition* pp 16133–16142 (IEEE, 2023).
206. Dosovitskiy, A. et al. An image Is worth 16×16 words: transformers for image recognition at scale. *ICLR 2021 — 9th Int. Conf. Learn. Represent.* (ICLR, 2021).
207. Arnab, A. et al. ViViT: a video vision transformer. *Proceedings of the IEEE/CVF International Conference on Compute Vision (ICCV)* pp 6816–6826 (IEEE, 2021).
208. Radford, A. Improving language understanding by generative pre-training. *Homol. Homotopy Appl.* **9**, 399–438 (2018).
209. Raffel, C. et al. Exploring the limits of transfer learning with a unified text-to-text transformer. *J. Mach. Learn. Res.* **21**, 1–67 (2020).
210. OpenAI. GPT-4 technical report. Preprint at *arXiv* http://arxiv.org/pdf/2303.08774 (2023).
211. Devlin, J., Chang, M. W., Lee, K. & Toutanova, K. in *Proceedings of the 2019 Conference of the North American Chapter of the Association for Computational Linguistics: Human Language Technologies* Vol. 1 (eds Burstein, J., Doran, C. & Solorio, T.) 4171–4186 (Association for Computational Linguistics, 2019).
212. Abdel-hamid, O. et al. Convolutional neural networks for speech recognition. *IEEE/ACM Trans. Audio Speech Lang. Process.* **22**, 1533–1545 (2014).
213. Sainath, T. N. et al. Deep convolutional neural networks for large-scale speech tasks. *Neural Netw.* **64**, 39–48 (2015).
214. Dong, L., Xu, S. & Xu, B. Speech-transformer: a no-recurrence sequence-to-sequence model for speech recognition. *Proceedings of the IEEE International Conference on Acoustics Speech and Signal Processing (ICASSP)* pp 5884–5888 (IEEE, 2018).
215. Baldi, P. Autoencoders, unsupervised learning, and deep architectures. *PMLR* **27**, 37–49 (2012).
216. Li, X., Wu, S. & Wang, L. Blood pressure prediction via recurrent models with contextual layer. *WWW'17: Proceedings of the 26th International Conference on World Wide Web* pp 685–693 (International World Wide Web Conferences, 2017).
217. Li, Y. H., Harfiya, L. N., Purwandari, K. & Lin, Y. D. Real-time cuffless continuous blood pressure estimation using deep learning model. *Sensors* **20**, 1–19 (2020).
218. Hochreiter, S. & Schmidhuber, J. Long short-term memory. *Neural Comput.* **9**, 1735–1780 (1997).

219. Hüsken, M. & Stagge, P. Recurrent neural networks for time series classification. *Neurocomputing* **50**, 223–235 (2003).
220. Su, P. et al. Long-term blood pressure prediction with deep recurrent neural networks. *Proceedings of the 2018 IEEE EMBS International Conference on Biomedical and Health Informatics* pp 323–328 (IEEE, 2018).
221. Mao, S. & Sejdic, E. A review of recurrent neural network-based methods in computational physiology. *IEEE Trans. Neural Netw. Learn. Syst.* **34**, 6983–7003 (2023).
222. Senturk, U., Yucedag, I. & Polat, K. Repetitive neural network (RNN) based blood pressure estimation using PPG and ECG signals. *Proceedings of the 2018 2nd International Symposium on Multidisciplinary Studies and Innovative Technologies (ISMSIT)* pp 1–4 (2018).
223. Park, S. R. & Lee, J. W. in *Proceedings of the 18th Annual Conference of the International Speech Communication Association: Interspeech 2017* (ed. Lacerda, F.) 1993–1997 (ISCA, 2017).
224. Shimazaki, S., Kawanaka, H., Ishikawa, H., Inoue, K. & Oguri, K. Cuffless blood pressure estimation from only the waveform of photoplethysmography using CNN. *Proceedings of the 2019 41st Annual International Conference of the IEEE Engineering in Medicine and Biology Society (EMBC)* pp 5042–5045 (IEEE, 2019).
225. Eom, H. et al. End-to-end deep learning architecture for continuous blood pressure estimation using attention mechanism. *Sensors* **20**, 2338 (2020).
226. Esmaelpoor, J., Hassan, M. & Kadkhodamohammadi, A. A multistage deep neural network model for blood pressure estimation using photoplethysmogram signals. *Comput. Biol. Med.* **120**, 103719 (2020).
227. Shi, Y., Yuan, W., Hu, S. & Lou, Y. Convolutional quasi-recurrent network for real-time speech enhancement. *J. Xidian Univ.* **49**, 183–190 (2022).
228. Zihlmann, M., Perekrestenko, D. & Tschannen, M. Convolutional recurrent neural networks for electrocardiogram classification. *Comput. Cardiol.* **44**, 1–4 (2017).
229. Keren, G. & Schuller, B. Convolutional RNN: an enhanced model for extracting features from sequential data. *Proceedings of the International Joint Conference on Neural Networks (IJCNN)* pp 3412–3419 (IEEE, 2016).
230. Mohiuddin, K. et al. Retention is all you need. *CIKM '23: Proceedings of the 32nd ACM International Conference on Information and Knowledge Management*.pp 4752–4758 (Association for Computing Machinery, 2023).
231. Celler, B. G., Le, P. N., Argha, A. & Ambikairajah, E. Blood pressure estimation using time domain features of auscultatory waveforms and GMM-HMM classification approach. *Annu. Int. Conf. IEEE Eng. Med. Biol. Soc.* **2019**, 208–211 (2019).
232. Sadrawi, M. et al. Genetic deep convolutional autoencoder applied for generative continuous arterial blood pressure via photoplethysmography. *Sensors* **20**, 3829 (2020).
233. Taniguchi, H. et al. in *Medical Image Computing and Computer-Assisted Intervention – MICCAI 2015* (eds Navab, N., Hornegger, J, Wells, M. W. & Frangi, A. F) 209–217 (Springer, 2015).
234. Athaya, T. & Choi, S. An estimation method of continuous non-invasive arterial blood pressure waveform using photoplethysmography: a U-net architecture-based approach. *Sensors* **21**, 1867 (2021).
235. Mahmud, S. et al. A shallow U-net architecture for reliably predicting blood pressure (BP) from photoplethysmogram (PPG) and electrocardiogram (ECG) signals. *Sensors* **22**, 919 (2022).
236. Mehrabadi, M. A., Aqajari, S. A. H., Zargari, A. H. A., Dutt, N. & Rahmani, A. M. Novel blood pressure waveform reconstruction from photoplethysmography using cycle generative adversarial networks. *Annu. Int. Conf. IEEE Eng. Med. Biol. Soc.* **2022**, 1906–1909 (2022).
237. Min, S. et al. Clinical validation of a wearable piezoelectric blood-pressure sensor for continuous health monitoring. *Adv. Mater.* **35**, e2301627 (2023).
238. Zhou, S. et al. Clinical validation of a wearable ultrasound sensor of blood pressure. *Nat. Biomed. Eng*. https://doi.org/10.1038/s41551-024-01279-3 (2024).
239. Kouz, K., Scheeren, T. W. L., De Backer, D. & Saugel, B. Pulse wave analysis to estimate cardiac output. *Anesthesiology* **134**, 119–126 (2021).
240. Qiu, S., Yan, B. P. Y. & Zhao, N. Stroke-volume-allocation model enabling wearable sensors for vascular age and cardiovascular disease assessment. *NPJ Flex. Electron.* **8**, 24 (2024).
241. Pollreisz, D. & TaheriNejad, N. Detection and removal of motion artifacts in PPG signals. *Mob. Netw. Appl.* **27**, 728–738 (2022).
242. Sayer, G. et al. Continuous monitoring of blood pressure using a wrist-worn cuffless device. *Am. J. Hypertens.* **35**, 407–413 (2022).
243. Trudeau, L. Central blood pressure as an index of antihypertensive control: determinants and potential value. *Can. J. Cardiol.* **30**, S23–S28 (2014).
244. Kim, J. S., Kim, D. W., Jung, H. T. & Choi, J. W. Controlled lithium dendrite growth by a synergistic effect of multilayered graphene coating and an electrolyte additive. *Chem. Mater.* **27**, 2780–2787 (2015).
245. Deng, R. & He, T. Flexible solid-state lithium-ion batteries: materials and structures. *Energies* **16**, 4549 (2023).
246. Gljušćić, P., Zelenika, S., Blažević, D. & Kamenar, E. Kinetic energy harvesting for wearable medical sensors. *Sensors* **19**, 4922 (2019).
247. Mo, X. et al. Piezoelectrets for wearable energy harvesters and sensors. *Nano Energy* **65**, 104033 (2019).
248. Zou, Y., Raveendran, V. & Chen, J. Wearable triboelectric nanogenerators for biomechanical energy harvesting. *Nano Energy* **77**, 105303 (2020).
249. Nozariasbmarz, A. et al. Review of wearable thermoelectric energy harvesting: from body temperature to electronic systems. *Appl. Energy* **258**, 114069 (2020).
250. Wang, Y. et al. Self-powered wearable pressure sensing system for continuous healthcare monitoring enabled by flexible thin-film thermoelectric generator. *Nano Energy* **73**, 104773 (2020).
251. Oh, Y. S. et al. Battery-free, wireless soft sensors for continuous multi-site measurements of pressure and temperature from patients at risk for pressure injuries. *Nat. Commun.* **12**, 5008 (2021).
252. Lin, R. et al. Wireless battery-free body sensor networks using near-field-enabled clothing. *Nat. Commun.* **11**, 444 (2020).
253. Ouyang, W. et al. A wireless and battery-less implant for multimodal closed-loop neuromodulation in small animals. *Nat. Biomed. Eng.* **7**, 1252–1269 (2023).
254. Li, J. et al. Thin, soft, wearable system for continuous wireless monitoring of artery blood pressure. *Nat. Commun.* **14**, 5009 (2023).
255. Ge, Y. et al. Contactless WiFi sensing and monitoring for future healthcare - emerging trends, challenges, and opportunities. *IEEE Rev. Biomed. Eng.* **16**, 171–191 (2023).
256. Enriko, I. K. A. & Gustiyana, F. N. Wi-Fi HaLow: literature review about potential use of technology in agriculture and smart cities in Indonesia. *Proceedings of the 2024 International Conference on Green Energy, Computing and Sustainable Technology (GECOST)* pp 277–281 (IEEE, 2024).
257. Yoo, J. Y. et al. Wireless broadband acousto-mechanical sensing system for continuous physiological monitoring. *Nat. Med.* **29**, 3137–3148 (2023).
258. Bai, L., Ciravegna, F., Bond, R. & Mulvenna, M. A low cost indoor positioning system using bluetooth low energy. *IEEE Access.* **8**, 136858–136871 (2020).
259. Selvan, S., Zaman, M., Gobbi, R. & Wong, H. Y. Recent advances in the design and development of radio frequency-based energy harvester for powering wireless sensors: a review. *J. Electromagn. Waves Appl.* **32**, 2110–2134 (2018).
260. Kwon, K. et al. A battery-less wireless implant for the continuous monitoring of vascular pressure, flow rate and temperature. *Nat. Biomed. Eng.* **7**, 1215–1228 (2023).
261. Boutry, C. M. et al. Biodegradable and flexible arterial-pulse sensor for the wireless monitoring of blood flow. *Nat. Biomed. Eng.* **3**, 47–57 (2019).
262. Smuck, M., Odonkor, C. A., Wilt, J. K., Schmidt, N. & Swiernik, M. A. The emerging clinical role of wearables: factors for successful implementation in healthcare. *NPJ Digit. Med.* **4**, 45 (2021).
263. Stergiou, G. S. et al. A universal standard for the validation of blood pressure measuring devices: Association for the Advancement of Medical Instrumentation/European Society of Hypertension/International Organization for Standardization (AAMI/ESH/ISO) Collaboration Statement. *Hypertension* **71**, 368–374 (2018).

Acknowledgements
The authors receive support from the National Research Foundation of Korea (NRF) by grants funded by the Korean government (MSIT; RS-2024-00406240 and RS-2023-00273231).

Author contributions
S.M., J.A., J.H.L. and J.H.K. researched data for the article; S.M., J.A., J.H.L. and S.H.E. wrote the manuscript; S.M., J.A., J.H.L., H.-S.A. and J.-Y.H. contributed to the discussion of its content; and K.J.L., D.J.J., C.D.Y., S.X. and J.A.R. reviewed or edited the manuscript before submission.

Competing interests
The authors declare no competing interest.

Additional information
Peer review information *Nature Reviews Cardiology* thanks Alberto Avolio and the other, anonymous, reviewer(s) for their contribution to the peer review of this work.

Publisher's note Springer Nature remains neutral with regard to jurisdictional claims in published maps and institutional affiliations.